Cortistatin exerts an immunomodulatory and neuroprotective role in a preclinical model of ischemic stroke

Castillo-González J[1], Buscemi L[2,3], Vargas-Rodríguez P[1], Serrano-Martínez I[1], Forte-Lago I[1], Price M[2,3], Hernández-Cortés P[4], Hirt L[2,3*], González-Rey E[1*].

[1]Institute of Parasitology and Biomedicine Lopez-Neyra (IPBLN), CSIC, PT Salud, 18016 Granada, Spain; [2]University of Lausanne, Lausanne, Switzerland; [3]Lausanne University Hospital, Lausanne, Switzerland; [4]Medicine School, University of Granada, Granada, Spain

*Correspondence: elena.g@csic.es; lorenz.hirt@chuv.ch; Tel.: +34-958-181670

Abstract

Ischemic stroke is the result of a permanent or transient occlusion of a brain artery, leading to irreversible tissue injury and long-term sequelae. Despite ongoing advancements in revascularization techniques, stroke remains the second leading cause of death worldwide. A comprehensive understanding of the complex and interconnected mechanisms, along with the endogenous mediators that modulate stroke responses is essential for the development of effective interventions. Our study investigates cortistatin, a neuropeptide extensively distributed in the immune and central nervous systems, known for its immunomodulatory properties. With neuroinflammation and peripheral immune deregulation as key pathological features of brain ischemia, cortistatin emerges as a promising therapeutic candidate. To this aim, we evaluated its potential effect in a well-established middle cerebral artery occlusion (MCAO) preclinical stroke model. Our findings indicate that the peripheral administration of cortistatin at 24 hours post-stroke significantly reduces neurological damage and enhances recovery. Importantly, cortistatin-induced neuroprotection was

multitargeted, as it modulated the glial reactivity and astrocytic scar formation, facilitated blood-brain barrier recovery, and regulated local and systemic immune dysfunction. Surprisingly, administration of cortistatin at immediate and early post-stroke time points proved to be not beneficial and even detrimental. These results emphasize the importance of understanding the spatio-temporal dynamics of stroke pathology to develop innovative therapeutic strategies. Premature interruption of certain neuroinflammatory processes might inadvertently compromise neuroprotective mechanisms. In summary, our study highlights cortistatin as a novel pleiotropic therapeutic approach against ischemic stroke, offering new treatment options for patients for whom early revascularization intervention is unsuccessful.

Graphical abstract

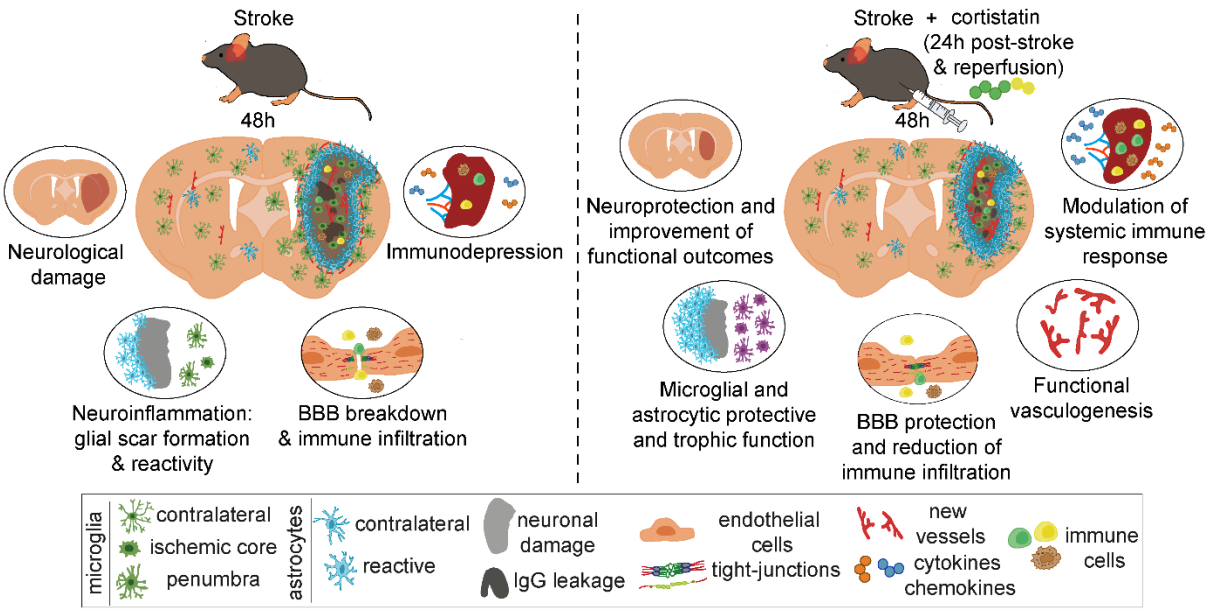

Keywords: blood-brain barrier breakdown, cortistatin, ischemic stroke, glial response, neuroimmune regulation, neuroinflammation, neuroprotection.

1. INTRODUCTION

Ischemic stroke results from a permanent or transient occlusion of a cerebral artery. The abrupt cessation of cerebral blood flow and subsequent reperfusion triggers a rapid and complex cascade of molecular and cellular events that may evolve over hours to days and weeks after the onset [1]. These pathophysiological events are diverse and include energy failure, oxidative stress, excitotoxicity, cell death, microglia reactivity, glial scar formation, blood-brain barrier (BBB) breakdown, and peripheral immune responses [2]. Notably, these processes are intricately interlinked, often unfolding concurrently within a brief time frame.

Despite significant efforts, stroke remains the second leading cause of death globally. Current treatments are limited to intravenous recombinant tissue plasminogen activator (rtPA) or endovascular thrombectomy. However, the narrow therapeutic window and rather limited efficacy sometimes restrict the utility of these treatments [3]. Furthermore, the intricate and still not fully understood spatiotemporal pathophysiology of stroke, with a plethora of underlying cellular and molecular processes involving the brain, vascular system, and peripheral organs, complicates its management. Consequently, there is an urgent need to thoroughly understand the neuroimmunological context and the factors involved at the different stages of ischemic pathology to develop effective therapeutic approaches.

Cortistatin (CST) is a cyclic neuropeptide broadly distributed in the central nervous system (CNS) and the immune system [4,5]. Despite sharing considerable homology, functions, and receptors (Sst1-5) with somatostatin, cortistatin exhibits unique functions in the nervous system and peripheral tissues [6,7]. These particular functions are mediated through interactions with receptors distinct from those of somatostatin, including the ghrelin receptor, the Mas gene-related receptor X-2, and a yet unidentified cortistatin receptor [5]. Notably, cortistatin displays potent anti-

65 inflammatory properties, protecting against the development and progression of
66 several inflammatory and autoimmune disorders (reviewed in [5]). Additionally,
67 cortistatin treatment demonstrates immunomodulatory and neuroprotective effects in
68 models of neuroinflammatory and neuroimmune disorders, such as multiple sclerosis
69 [8], meningoencephalitis [9], excitotoxicity [10], neuropathic pain [11], and Parkinson's
70 disease [12]. In these conditions, cortistatin consistently reduces pro-inflammatory
71 mediators, modulates glial cell responses, and maintains tissue-surveillance activities.
72 Importantly, the absence of cortistatin in mice is associated with an exacerbated pro-
73 inflammatory basal state in the CNS and periphery, along with decreased expression
74 of neurotrophic factors [5,8]. Recently, our group has demonstrated a key role for
75 cortistatin in maintaining BBB integrity, mediating anti-inflammatory endothelial
76 functions, and facilitating BBB repair by stabilizing tight-junction proteins (TJs) and
77 mitigating exaggerated immune responses after ischemic-like *in vitro* conditions [13].
78 However, no data has been reported about the influence of cortistatin on *in vivo*
79 ischemic damage.

80 Therefore, given its neuroprotective, anti-inflammatory, and immunomodulatory
81 properties, as well as its ability to regulate the BBB, we hypothesize that cortistatin
82 could be a promising therapeutic agent affecting the intricate glial, vascular and
83 peripheral responses underlying stroke pathophysiology.

84 2. MATERIALS AND METHODS

85 *2.1. Peptides*

86 Mouse CST-29 was acquired from Bachem. The lyophilized peptide was dissolved in
87 distilled water (final concentration 10^{-4} M).

88 *2.2. Animals*

89 The procedures described in this study were approved by the Animal Care and Use
90 Board and the Ethical Committee of the Spanish National Research Council (Animal
91 Care Unit Committee IPBLN-CSIC # protocol CEEA OCT/2017.EGR), and the Vaud
92 Cantonal Veterinary Office (protocol number 2017x6a) (Switzerland). All experimental
93 protocols adhered to the guidelines specified in Directive 2010/63/EU of the European
94 Parliament and the corresponding Swiss regulations regarding animal protection for
95 scientific purposes. Mice were housed in groups of five animals per cage under
96 controlled environmental conditions (60-70% relative humidity, 22 ± 1°C), and
97 maintained on a 12-hour light/dark cycle (lights on at 7:00 a.m.). Food and water were
98 provided *ad libitum*.

99 ### *2.3. Transient middle cerebral artery occlusion model*

100 Cerebral ischemia was induced in 12-week-old male C57BL/6J mice using the
101 transient middle cerebral artery occlusion (MCAO) model, as adapted from Buscemi
102 et al. [14]. Briefly, mice were anesthetized with isoflurane (1.5-2% in 70% N_2O/30%
103 O_2) using a facemask. For post-surgical analgesia buprenorphine (0.025 mg/kg) was
104 subcutaneously administered. A heating pad was used to maintain body temperature
105 throughout the surgery. Regional cerebral blood flow (CBF) was monitored using laser
106 Doppler flowmetry (moorVMS-LDF1, Moor Instruments) by fixing a probe on the skull
107 over the core area supplied by the middle cerebral artery (approximately 1mm
108 posterior and 6mm lateral from the bregma). Transient focal ischemia was induced by
109 introducing a silicon-coated filament (701756PK5Re, Doccol) through the left common
110 carotid artery into the internal carotid artery until it occluded the middle cerebral artery.
111 The filament was left in place for 20 minutes before being withdrawn to allow
112 reperfusion. Surgeries were considered successful when blood dropped below 20%
113 of the baseline during occlusion, and raised above 50% of the baseline after filament

114 withdrawal. Post-surgery, mice were housed with *ad libitum* access to food and water,
115 with each cage containing water-softened chow and recovery gel.

116 Cortistatin (144µg/kg) was administered intraperitoneally at 0h and 24h
117 (immediate treatment), 4h and 24h (early treatment), or 24h (late treatment) post-
118 reperfusion. Control mice received an equivalent volume of saline solution.

119 ***2.4. Neurological score and behavioural tests***

120 Neurological assessments were conducted at 24h following MCAO and prior to
121 sacrifice at 48h. Stroke severity was assessed on a scale from 0 (no signs) to 3 (death)
122 determining motor, balance, reflex, and sensory functions using a compendium of
123 scales previously published [15,16].

124 To evaluate motor function and ataxia, the rotarod test was performed using a
125 rotating cylinder apparatus (Ugo Basile, Gemonio, Italy) with a gradual acceleration
126 protocol. The cylinder accelerated from 4rpm to 40rpm over 216s and then maintained
127 a constant speed of 40rpm until reaching a 300s time limit. To ensure reliable results
128 and exclude motivational factors, such as early falls, a training phase was conducted
129 [17]. Mice underwent three consecutive daily training trials (with a 10-minute gap
130 between them) for two days before MCAO (training trials, baseline). The longest
131 latency to fall from the rod in three trials was recorded for each mouse. Mice underwent
132 daily test trials at 24h and 48h after MCAO. For the test trials, the longest latency to
133 fall from the rod or to complete two consecutive full turns while gripping the rod within
134 the 300 seconds time limit was recorded for each mouse.

135 Additionally, muscle coordination and endurance were assessed using the wire-
136 hanging test. Animals were suspended on a custom-made apparatus consisting of a
137 single wire stretched between two posts above a soft ground. Mice were trained 24h

138 before surgery and scored based on their performance in scaping (touching and
139 reaching either the right or left post) or falling at 24 hours and 48 hours after MCAO
140 [15]. The time elapsed until they escaped or fell was recorded. The test concluded
141 either after 180 seconds or when a mouse had fallen off the wire ten times.

142 ### *2.5. Sacrifice and infarct volume measurement*

143 Mice were euthanized by intraperitoneal injection overdose of ketamine (100mg/kg,
144 Ritcher Pharma)/ xylazine (10mg/kg, Fatro Iberica) at 48h post-MCAO surgery,
145 followed by intracardial perfusion with 4% paraformaldehyde (PFA). Brains were
146 collected and post-fixed in 4% PFA for 24h at 4°C, and then cryoprotected in 30%
147 sucrose for 48h at 4°C. Subsequently, brains were frozen in isopentane on dry ice at
148 -25°C and stored at -80°C until further processing. Coronal sections of 20µm thickness
149 were obtained using a cryostat.

150 Cresyl violet (CV)-stained sections were prepared by gradual hydration in
151 ethanol, stained with 1mg/ml of CV-acetate in distilled water, gradual dehydration in
152 ethanol, and clearing in xylene [15]. Sections were imaged under a Leica DM2000
153 Transmit stereomicroscope at 2.5x magnification. The infarct volume was determined
154 by multiplying the sum of the infarcted areas on each section (measured using the
155 ImageJ Fiji software) by the section spacing.

156 ### *2.6. Immunofluorescence*

157 For immunofluorescence labelling, 20µm free-floating sections were washed with PBS
158 and blocked and permeabilized with PBS containing 1% BSA, 0.1% Triton X-100, and
159 5% goat serum for 60min at room temperature (RT). Following this, sections were
160 incubated overnight (O/N) at 4°C with primary antibodies anti-MAP2 (1:1000, Sigma),
161 anti-Iba1 (1:1000, Wako), anti-GFAP (1:5000, Dako), anti-CD31/PECAM-1 (1:300,

162 BD), anti-ZO-1 (1:100, Fisher), or APC-labelled anti-CD45 (1:200, BD) in PBS
163 containing 1% BSA, 0.1% Triton X-100, and 5% goat serum. After extensive washing
164 with PBS, sections were incubated with the corresponding secondary Alexa Fluor-
165 conjugated antibodies (1:1000, Sigma) and DAPI in PBS containing 1% BSA, 0.1%
166 Triton X-100, and 2% goat serum for 60min. Sections were mounted with Mowiol. For
167 IgG staining, an Alexa Fluor 594-conjugated goat anti-mouse IgG antibody was utilized
168 without a primary antibody. Images were captured using a LEICA DMi8 S Platform
169 Life-cell microscope at 20x magnification and a confocal Leica TCS SP8 STED
170 microscope at 63x magnification.

171 ### *2.7. Morphometric characterization*

172 To comprehensively characterize morphological alterations in microglia and
173 astrocytes post-stroke, we employed different morphometric analyses. Images of
174 selected microglia and astrocytes within specific brain regions (*i.e.,* periinfarct or core
175 area) were randomly selected, ensuring no overlap between cells, and that the entire
176 nucleus and branches were included. A total of 15-30 cells per mouse (n=15-30) from
177 3-6 mice (N=3-6) were analysed. Image processing was conducted using ImageJ Fiji
178 software, following a systematic protocol adapted from others [12,18,19]. Images were
179 converted to 8-bit grayscale, pre-processed to minimize background noise and
180 enhance contrast, and binarized by applying a pre-established threshold. Extraneous
181 pixels not corresponding to cells were eliminated using the *Remove outliers* and
182 *Despeckle* tools, with manual editing performed as necessary to address significant
183 background noise.

184 Following image pre-processing, the Skeleton and Fractal Analysis plugins of
185 ImageJ Fiji software [20] were used. Specific parameters assessed included the
186 number of junctions (Skeleton Analysis) and the convex hull area (*i.e.,* the area

187 containing the entire cell shape enclosed by the smallest convex polygon), fractal
188 dimension (*i.e.,* index of complexity), span ratio (*i.e.,* the ratio of the axes of the convex
189 hull from major to minor), and circularity (*i.e.,* how closely the shape of an object
190 resembles a circle) (Fractal Analysis). For detailed procedures, refer to the user
191 manual of the respective plugins [20].

192 ### *2.8. Determination of the peripheral immune response*

193 To evaluate the peripheral immune response, we determined the levels of systemic
194 immune mediators and the spleen cellularity. First, to quantify the levels of peripheral
195 inflammatory factors, blood samples were collected by cardiac puncture, allowed to
196 clot for 2h at RT, and then centrifuged at 2,000rpm for 10min. The concentration of
197 inflammatory mediators in the serum was determined by sandwich ELISA assay.
198 Briefly, maxisorb plates (Millipore) were coated O/N at 4°C with the capture antibodies
199 (anti-IL-6, anti-IL-12 from BD Pharmigen, or anti-MCP-1 from PeproTech). The plates
200 were then washed with PBS containing 0.05% Tween20 and blocked with PBS
201 containing 10% FBS for 2h. The samples and the recombinant standards were added
202 to the plates and incubated O/N at 4°C. Following incubation, biotinylated detection
203 antibodies (Serotec) were added for 1h at RT. After washing, plates were incubated
204 with avidin-HRP (Sigma) (1:500 in blocking buffer) for 1h and then developed with
205 ABTS substrate (Sigma). Absorbance was measured at 405nm using a
206 spectrophotometer (Molecular Devices) and concentrations of inflammatory factors
207 were determined based on the standard curve generated simultaneously.

208 Next, spleens were collected and weighed. Spleen tissue was gently ground
209 with the frosted part of two slides onto a 100mm culture dish. The homogenized tissue
210 was then transferred to RPMI medium supplemented with 10% FBS, 2mM L-
211 glutamine, 1% P/S, and 50μM 2-mercaptoethanol. After allowing the suspension to sit

212 for 5min on ice, the cell suspension was carefully collected and centrifuged at
213 1,670rpm for 10min at 4°C. To the resulting pellet, Ack buffer (150mM NH_4Cl, 10mM
214 $KHCO_3$, 0.1mM Na_2EDTA) was subsequently added for 10min at RT to lyse red blood
215 cells. Next, RPMI medium was added, and cells were centrifuged at 1,670rpm for
216 10min at RT and counted.

217 ### *2.9. RNA extraction and evaluation of gene expression*

218 Following MCAO, brains were collected and divided into the contralateral and
219 ipsilateral sides in both control and cortistatin-treated mice. For RNA isolation, brain
220 tissues were placed in TriPure reagent (Roche). Then, cDNA synthesis was carried
221 out using the RevertAid First Strand cDNA Synthesis Kit (ThermoFisher) with random
222 hexamers in a CFX Connect QPCR System (Biorad) under the following conditions:
223 incubation at 25°C/5 min, reverse transcription at 42°C/60 min, inactivation at 70°C/5
224 min. Gene expression analysis was conducted using conventional qPCR. SensiFast
225 Sybr No-Rox kit 1x (Bioscience) was added to the cDNA corresponding to 20ng of
226 RNA, along with the corresponding reverse and forward primers for each gene, and
227 nuclease-free water to a final volume of 20µl. The CFX96 thermocycler (BioRad) was
228 used to conduct the reaction under the following conditions: 94°C/5min (polymerase
229 activation) followed by 40 cycles at 94°C/30s (denaturalization), 58°C/60°C/62°C/30s
230 (primer annealing temperature depending on the gene), and 72°C/30s (extension).
231 The comparative threshold cycle (Ct) method was performed for quantification. Each
232 gene Ct values were normalized to those of the housekeeping gene *Rplp0* within each
233 PCR reaction. Fold change was determined using the ΔΔCt method. The specific
234 primers for each gene are provided in Additional file 1: Tables S1.

235 ### *2.10. Statistical analysis*

236 Data are presented as the mean ± SEM. All experiments were conducted in a blinded
237 and randomized manner. The number of independent animals (N), and tissue sections
238 and cell types (n) are indicated. Statistical differences between two groups were
239 conducted using the unpaired Student's t test for normal distribution and parametric
240 data, or the non-parametric Mann-Whitney U-test. For comparing three or more groups
241 that display normal distribution and parametric data, one-way ANOVA with Fisher´s
242 LSD test *post-hoc* tests for multiple comparisons was conducted. Three or more
243 groups that display non-parametric data were evaluated by Kruskal-Wallis test with an
244 uncorrected Dunn *post-hoc* test. Brown-Forsythe and Welch ANOVA with unpaired t-
245 test and Welch´s correction *post-hoc* test were performed in the case standard
246 deviations were not assumed to be equal. All statistical analyses were performed using
247 GraphPad Prism v8.3.0 software, with P-values < 0.05 (one-tailed) considered
248 statistically significant.

249 **3. RESULTS**

250 ***3.1. Identification of the optimal administration time of cortistatin in an***
251 ***acute stroke model***

252 To investigate the potential therapeutic effect of the neuropeptide in ischemic stroke,
253 we chose the MCAO model, a well-established preclinical model that closely mimics
254 the human ischemic condition [21]. To consider the different phases of the pathology
255 [2], we first administered cortistatin across different temporal contexts during stroke
256 progression (Fig. 1A).

257 We administered the neuropeptide at three distinct time points: immediately
258 post-MCAO (0h and 24h post-reperfusion), early post-MCAO (4h and 24h post-
259 reperfusion), and late post-MCAO (24h post-reperfusion). The immediate treatment

260 aimed to influence neuroinflammatory and neurodegenerative responses immediately
261 after ischemia. The early treatment targeted pathological processes occurring within
262 the first hours after hypoxia-reperfusion, while the late treatment focused on processes
263 already established during the acute phase of stroke.

264 To determine the effect of cortistatin, we assessed neurological scores,
265 behavioural impairments, and brain damage in C57BL/6J mice after administering
266 cortistatin at the specified time points. First, neurological deficits resulting from stroke
267 were evaluated within 24-48h after MCAO using a neurological scoring system
268 encompassing motor, balance, reflex, and sensory functions graded from 0 to 3
269 (modified from [15]). As shown in Fig. 1B, MCAO control mice (saline-treated)
270 exhibited a mean score of 0.5-1, indicating minor motor incoordination and slight
271 hypomobility. Immediate cortistatin treatment significantly worsened neurological
272 scores to 1-2, related to moderate intermittent circling, tremor twitches, and motor
273 incoordination. However, early and late treatments did not significantly alter the
274 neurological score compared to controls, despite the significant reduction in lesion size
275 with late treatment (Fig. 1E,F).

276 We further evaluated motor function and muscle coordination using the rotarod
277 and wire-hanging tests (Fig. 1C,D; Supplementary Fig. 1). In both tests, mice
278 performance was measured 24h before the surgery (baseline, BL), and at 24 and 48h
279 post-surgery.

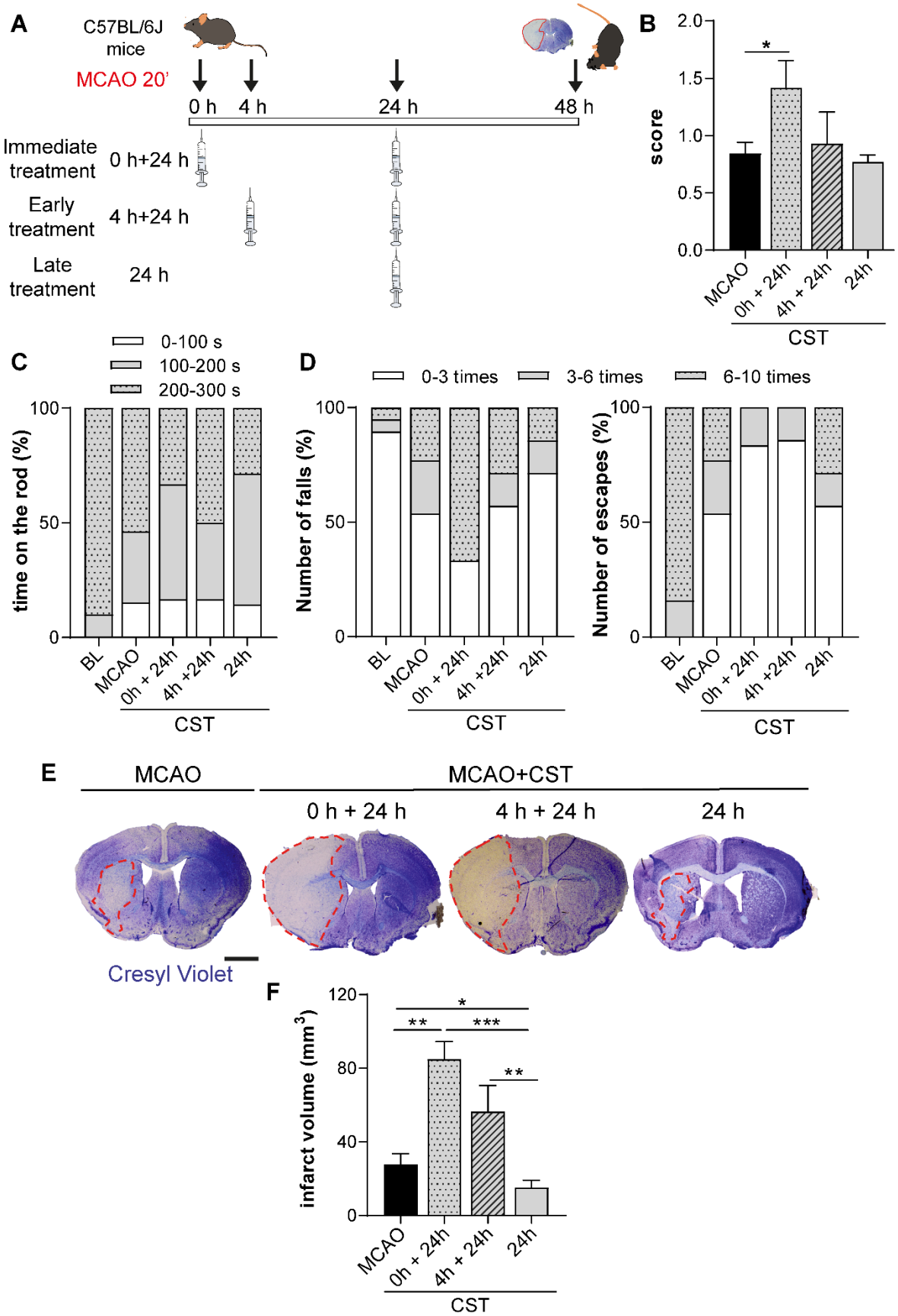

Fig. 1. Optimization of the administration time of cortistatin in a preclinical stroke model. A. Schematic representation of the experimental timeline. C57BL/6J mice were subjected to MCAO and

received either a saline solution (MCAO) or cortistatin (144µg/kg; MCAO+CST) at three distinct time intervals: immediately following reperfusion (0h + 24h), early after reperfusion (4h + 24h), and at late time post-reperfusion (24h). **B.** Neurological scores at 48h were assessed on a scale from 0 (no signs) to 3 (death). **C,D.** Behavioural performances were assessed by rotarod and wire-hanging tests, both at baseline (BL, pre-MCAO) and 48h post-MCAO. The time on the rod was evaluated in the rotarod test (**C**). In the wire-hanging test (**D**), the number of falls (**left**) and escapes (**right**) toward one of the posts were evaluated. Data are represented as the percentage of the total values based on the legend classification. N = 6-13 mice/group. **E.** Representative coronal brain sections from mice treated with either saline or CST at the specified times, stained with cresyl violet (CV). Ischemic lesions are outlined with dashed red lines. Scale bar: 1500µm **F.** Ischemic volume across the brain was determined by measuring ten CV-stained brain slices at 2-mm intervals per mouse. Data are expressed as mean ± SEM. **vs.* MCAO-saline treated mice, $*p \leq 0.05$, $**p \leq 0.01$, $***p \leq 0.001$. CST: cortistatin, MCAO: middle cerebral artery occlusion.

As expected, both tests showed worsened performance in MCAO mice at 24h-48h post-surgery compared to BL (Fig. 1C,D, Supplementary Fig. 1). Specifically at 48h, saline-treated MCAO mice displayed a reduced time on the rod compared to BL (46.2% lasting less than 200 seconds *vs.* 90% of mice performing beyond this time point at BL), which was similar in the early treatment but reduced with the immediate cortistatin administration (50% and 71.4% of mice falling before 200 seconds, respectively) (Fig. 1C; Supplementary Fig. 1A). In the wire-hanging test, stroke control mice displayed a worsened performance and increased number of falls (only 53.8% falling less than 3 times *vs.* 89.5% of BL, and only 23.1% escaping more than 6 times *vs.* 84.2% of BL) (Fig. 1D, Supplementary Fig. 1B). Immediate treatment resulted in poorer performance compared to saline and other treatments (66.6% falling more than 6 times *vs.* 23.1% saline, and 83.3% escaping less than 3 times *vs.* 53.8% saline) (Fig. 1D, Supplementary Fig. 1B,C). Early treatment also showed similar trends in performance metrics (Fig. 1D, Supplementary Fig. 1C). However, although late treatment showed no beneficial effect on the rotarod test, it improved performance in the wire-hanging assay, with fewer animals falling more than 6 times compared to saline and other treatments (14.3% vs. 23.1% saline) (Fig. 1D, Supplementary Fig. 1B,C). Similarly, the percentage of animals escaping more than 6 times increased

314 (28.6% vs. 23.1% saline or 0% for the other treatments) (Fig. 1D, Supplementary Fig.
315 1B,C).

316 Next, neurological lesions were quantified using CV staining, which
317 differentiates intact neuronal cytoplasm (intense purple), from infarcted areas with
318 dead neurons (faded purple) [22]. We observed that mice treated immediately after
319 MCAO displayed larger infarct volumes when compared to MCAO controls (Fig. 1E,F).
320 Remarkably, this treatment caused significant damage in the cortex and the striatum,
321 spreading to the hippocampus area (data not shown), consistent with the observed
322 worsened scores. Early treatment also led to larger lesions compared to MCAO-saline
323 mice but to a lesser extent than the immediate treatment (Fig. 1E,F). In contrast, late
324 treatment with cortistatin significantly decreased infarct volume, with only 23% of mice
325 treated at 24h showing infarct volumes above 20mm³, compared to 44% of controls,
326 100% of immediately treated mice, and 66% of early-treated mice (Figure 1C,F).

327 ***3.2. Differential time administration of cortistatin affects stroke-derived***
328 ***glial responses***

329 To investigate the underlying mechanisms by which cortistatin might differentially
330 affect ischemic lesions and neurological deficits when administered at different times,
331 we analysed the local neuroinflammatory response. In ischemic stroke, microglia are
332 very early responders. These cells swiftly migrate to the infarct core, proliferating and
333 adopting an amoeboid phenotype to engulf dead neurons [23]. Interestingly,
334 immediate and early treatment with cortistatin resulted in reduced microglia density in
335 the ischemic core compared to MCAO controls, while late treatment increased
336 microglia density, potentially indicating a more physiological response to the injury
337 (Fig. 2A,B).

338 Since morphological alterations in microglia closely correlate with their reactivity
339 states and serve as indicators of the severity of brain injury [18,24], we conducted
340 Skeleton Analysis to evaluate microglia morphotypes. In the infarct core, microglia in
341 saline-treated MCAO mice displayed a typical reactive amoeboid-like shape (Fig.
342 2C,D). Remarkably, immediate treatment with cortistatin led to a more pronounced
343 reactive phenotype than controls, characterized by fewer junctions, and larger area.
344 Conversely, early treatment resulted in a phenotype similar to MCAO mice, but with
345 an increased number of ramifications, while late treatment was associated with an
346 increased number of junctions and a significantly reduced soma, suggesting a
347 transition to a less ameboid microglia state (Fig. 2C,D).

348 Microglia in the ischemic penumbra also undergo intricate morphological and
349 functional changes [25]. We observed that immediate and early treatments increased
350 the number of junctions and overall microglial size, indicating a hyper-ramified
351 morphotype that was particularly pronounced in the early treatment. In contrast, late
352 treatment resulted in smaller soma sizes, while the number of junctions and microglia
353 area were similar to those in the MCAO control group, suggesting a different reactive
354 state (Fig. 2E,F).

355

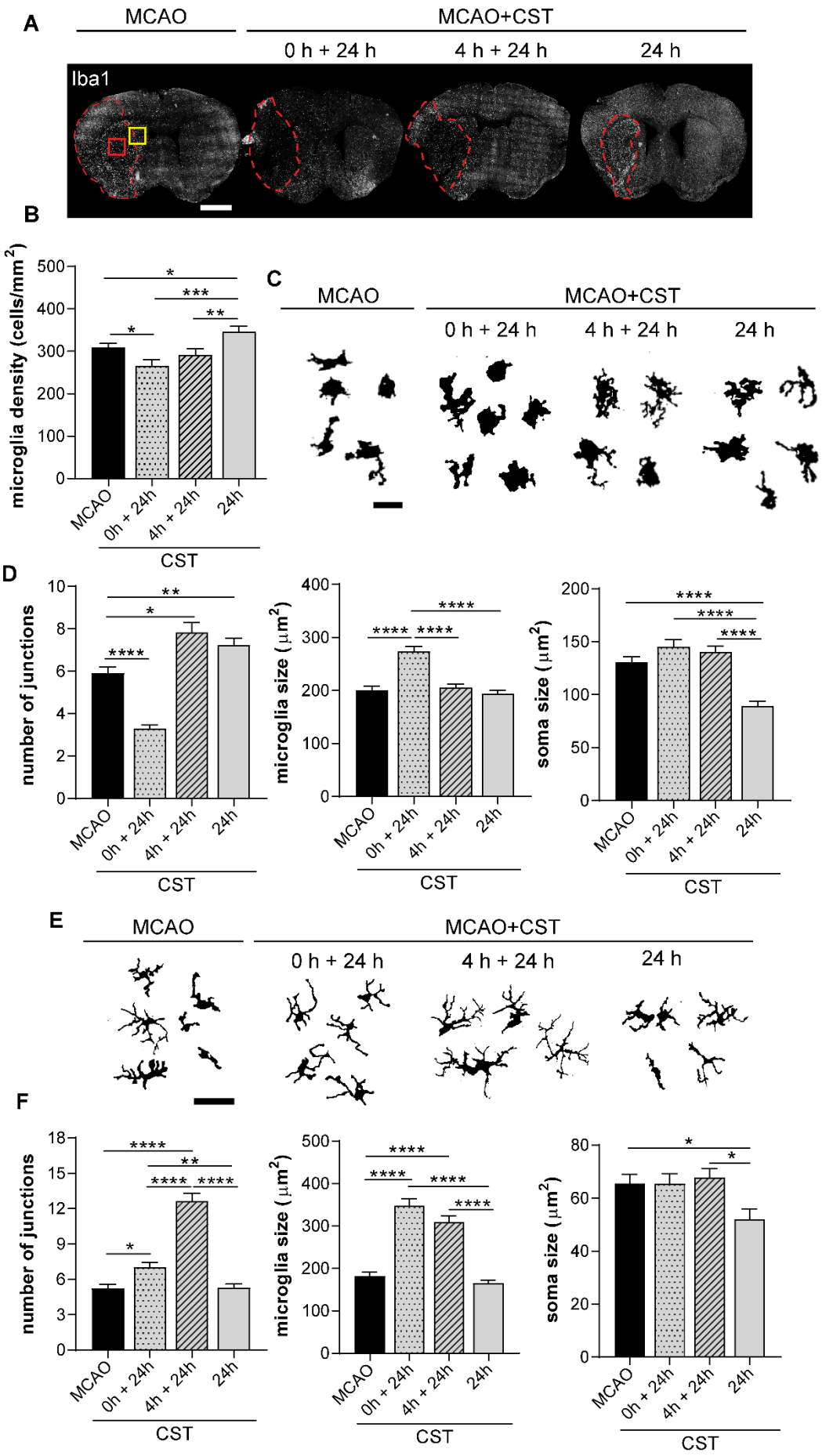
A
MCAO
MCAO+CST
0 h + 24 h
4 h + 24 h
24 h
Iba1
B
microglia density (cells/mm2)
500
400
300
200
100
0
*
***
**
*
MCAO
0h + 24h
4h + 24h
24h
CST
C
MCAO
MCAO+CST
0 h + 24 h
4 h + 24 h
24 h
D
number of junctions
10
8
6
4
2
0
**
*
****
MCAO
0h + 24h
4h + 24h
24h
CST
microglia size (μm2)
400
300
200
100
0
****
**** ****
MCAO
0h + 24h
4h + 24h
24h
CST
soma size (μm2)
200
150
100
50
0
****
****
****
MCAO
0h + 24h
4h + 24h
24h
CST
E
MCAO
MCAO+CST
0 h + 24 h
4 h + 24 h
24 h
F
number of junctions
18
15
12
9
6
3
0
****
**
**** ****
*
MCAO
0h + 24h
4h + 24h
24h
CST
microglia size (μm2)
500
400
300
200
100
0
****
****
****
****
MCAO
0h + 24h
4h + 24h
24h
CST
soma size (μm2)
80
60
40
20
0
*
*
MCAO
0h + 24h
4h + 24h
24h
CST

356

357 **Fig. 2. Time-dependent cortistatin treatment differentially regulates microglia response after**
358 **stroke. A.** Brain coronal sections of C57BL/6J mice were obtained after MCAO and subsequent
359 treatment with either saline solution (MCAO) or cortistatin (144µg/kg; MCAO+CST) at three distinct time
360 intervals: immediately following reperfusion (0h + 24h), early after reperfusion (4h + 24h), and at a late
361 time post-reperfusion (24h). Microglia was identified by Iba1 staining. The ischemic core is represented
362 by dashed red lines. Scale bar: 1,500µm. **B.** Density of microglia (cells/mm^2) was measured in the
363 ischemic core in the above-mentioned mice. **C-E**. Representative binary microglia from the different
364 experimental groups from the ischemic core (red square) (**C**), or the penumbra (yellow square) (**E).**
365 Scale bar: 30µm. Morphological parameters analysed (**D,F**). Skeleton Analysis was used to assess the
366 number of junctions (**D,F** left panel). Cell area (**D,F** middle panel) and soma size (**D,F** right panel) were
367 manually measured. n = 15-20 cells/mice; N = 3 mice/group. Data represent the mean ± SEM. **vs.*
368 saline *$p \leq 0.05$, **$p \leq 0.01$, ***$p \leq 0.001$, ****$p \leq 0.0001$. CST: cortistatin, Iba1: ionized calcium-binding
369 adaptor molecule 1, MCAO: middle cerebral artery occlusion.

370 Parallel to the microglia response, astrocytes also become reactive and
371 establish a glial scar surrounding the wound, containing the injury and preventing its
372 expansion to adjacent still-viable regions [26] (Fig. 3A)

373 Remarkably, our study found that the immediate cortistatin treatment impaired
374 glial scar formation, resulting in decreased scar thickness when compared to MCAO
375 control mice. Nevertheless, early and especially late treatments significantly increased
376 glial scar formation (Fig. 3A,B). Of note, the disorganized glial scar in the immediate
377 treatment match with the severe neuronal lesion and the reduced microglial density in
378 the core (Fig. 1E,F; 2B). We further analysed astrocyte morphology using Skeleton
379 Analysis to explore the influence of cortistatin treatment in the astrocytic response.
380 While astrocytes from MCAO mice displayed a high number of junctions, immediate
381 treatment resulted in a significant reduction, suggesting a more quiescent astrocytic
382 phenotype (Fig. 3C,D). Astrocytes from mice with early treatment were similar to the
383 saline-treated MCAO mice, while late treatment showed astrocytes with reduced
384 junctions and area, but increased soma size (Fig. 3C,D), suggesting a distinct reactive
385 phenotype, which can be linked to the enhanced glial scar formation (Fig. 3A,B).

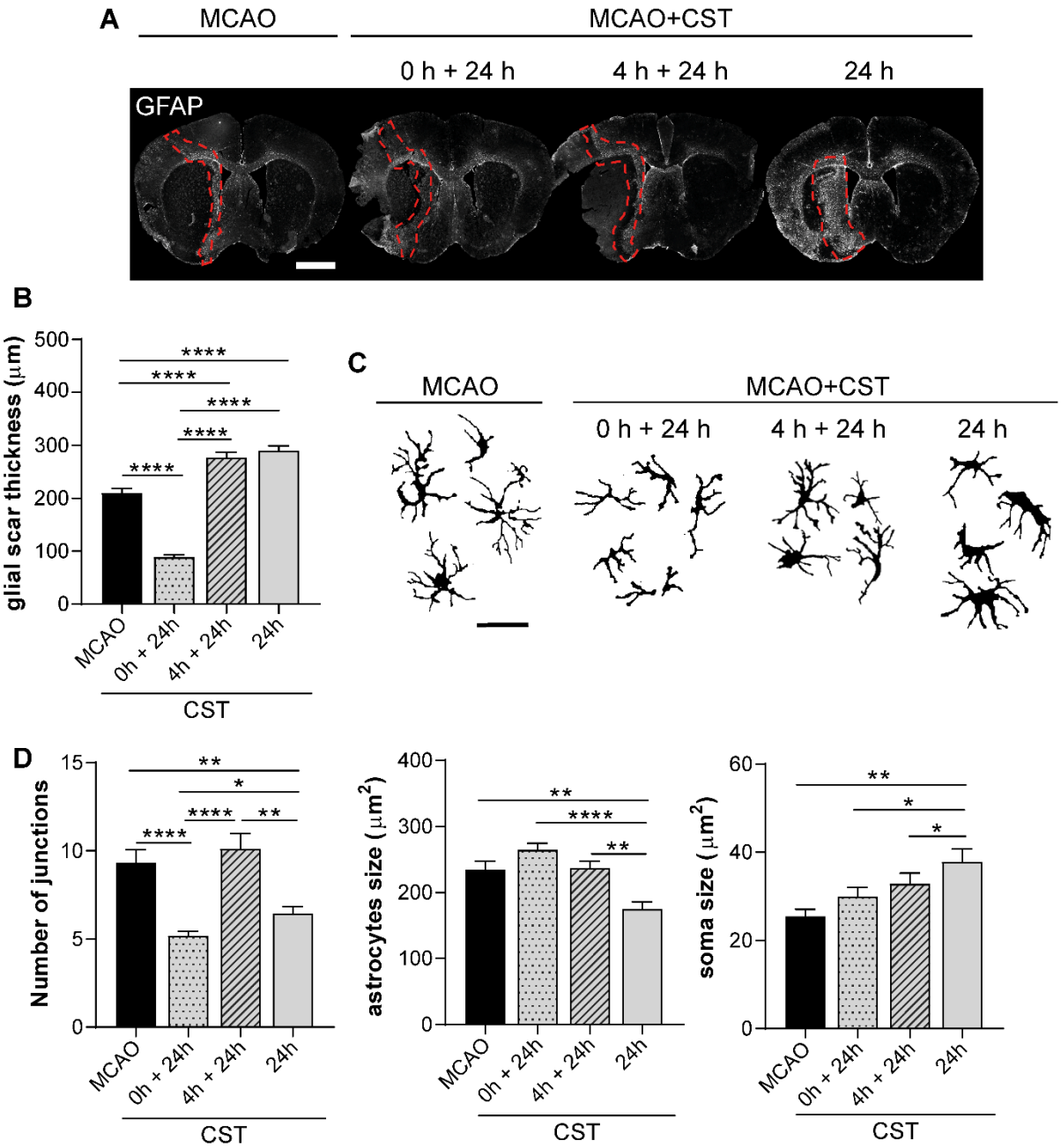

386

387 **Fig. 3. Time-dependent cortistatin treatment differentially impacts astroglial scar formation. A.**
388 Brain coronal sections of C57BL/6J mice were obtained after MCAO and subsequent treatment with
389 either saline solution (MCAO) or cortistatin (115µg/kg; MCAO+CST) at three distinct time intervals:
390 immediately following reperfusion (0h + 24h), early after reperfusion (4h + 24h), and at a late time post-
391 reperfusion (24h). Astrocytes were identified by GFAP staining. Glial scar is outlined with dashed red
392 lines. Scale bar: 1,500 µm. **B.** Glial scar thickness was quantified. N = 4-6 mice/group. **C.**
393 Representative images of astrocytes in binary were extracted from the glial scar in the different
394 experimental groups. Scale bar: 30µm. **D.** Evaluation of morphological parameters of astrocytes.
395 Number of junctions (**D,** left panel) was evaluated by Skeleton Analysis. Cell (**D.** middle panel) and
396 soma size (**D,** right panel) were manually measured. n = 15-20 cells/mice; N = 3 mice/group. Data are
397 presented as the mean ± SEM. *$vs.$ saline, *$p \leq 0.05$, **$p \leq 0.01$, ***$p \leq 0.001$, ****$p \leq 0.0001$. CST:
398 cortistatin, GFAP: glial fibrillary acidic protein, MCAO: middle cerebral artery occlusion.

399 Collectively, these results suggest that during the hyperacute stroke phase, the
400 initial glial response may be partially or fully deactivated by the potent anti-
401 inflammatory effects of the neuropeptide when administered immediately or early. This
402 deactivation leads to diminished protection of the damaged area, exacerbating
403 neuronal lesions and motor deficits. In contrast, late cortistatin administration
404 modulates the neuroinflammatory response differently, regulating glial cell
405 hyperreactivity and/or proliferation, which results in reduced neuronal lesions and
406 improved outcomes.

407 ***3.3. Treatment with cortistatin at later stages of ischemic stroke exerts***
408 ***neuroprotective effects***

409 Based on these findings, we conducted a detailed investigation into the effects of
410 cortistatin administered at 24h on neurodegeneration, glial population, BBB integrity,
411 brain vasculature alterations, and local as well as peripheral immune responses at 48h
412 following MCAO.

413 Our initial observations revealed that cortistatin-treated mice display reduced
414 area of neuronal damage in both cortex and striatum compared to MCAO mice, as
415 evidenced by MAP-2 neuronal staining (Fig. 4A,B), which was consistent with CV
416 staining (Fig. 1E,F). Notably, ischemic injury coincided with decreased expression of
417 neurotrophic factors such as BDNF and GDNF. Following treatment with cortistatin,
418 the levels of these factors were significantly restored to baseline levels (Fig. 4C).

419

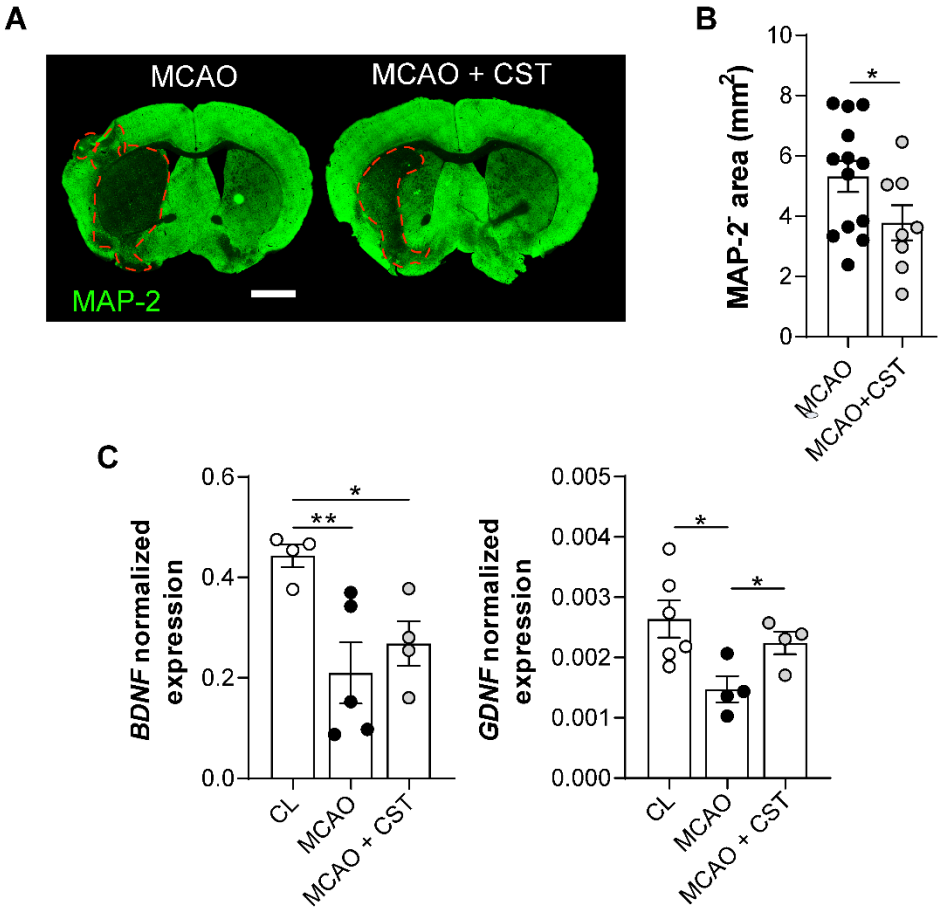

Fig. 4. Late administration of cortistatin promotes neuroprotection. **A**. Brain coronal sections from C57BL/6J mice subjected to MCAO and treated with either saline (MCAO) or cortistatin (144µg/kg) (MCAO+CST) at 24 hours post-reperfusion and sacrificed at 48 hours. Sections were stained with MAP-2 to visualize neurons. Ischemic lesions, corresponding to a lack of MAP-2 staining, are delineated with dashed red lines. Scale bar: 1,500µm. **B**. Quantification of the ischemic lesion area. N = 13 (MCAO), 8 (MCAO+CST) mice/group. **C**. Gene expression levels in the contralateral (CL, uninjured) and ipsilateral (ischemic) brain hemispheres of mice treated with saline or cortistatin following MCAO were analysed by real-time qPCR and normalized to *Rplp0* expression. N = 4-6 mice/group. Data are presented as mean ± SEM with dots representing individual mice. **vs.* saline, *$p \leq 0.05$, **$p \leq 0.01$. BDNF: brain-derived neurotrophic factor, CST: cortistatin, GDNF: glial cell line-derived neurotrophic factor, MAP-2: microtubule-associated protein 2, MCAO: middle cerebral artery occlusion.

3.4. Late treatment with cortistatin induces a neuroprotective microglial response in the acute stroke model

Next, we aimed to delve deeper into the role of cortistatin in modulating microglial morphotypes and functions, particularly focusing on its impact when administered at a later time post-stroke. To this aim, we complemented our initial morphometric analysis with a Fractal Analysis to evaluate various complexity parameters of microglia

438 from the ischemic core and penumbra in MCAO mice treated with cortistatin (Fig.5;
439 Supplementary Fig.2).

440 MCAO animals exhibited a reactive microglial phenotype in the ischemic
441 penumbra, characterized by a smaller territory area, enhanced complexity (as
442 indicated by span ratio and fractal dimension), and decreased circularity compared to
443 contralateral microglia (Fig. 5B,C). However, treatment with cortistatin seemed to
444 mitigate this reactivity, evidenced by reductions in the soma size, junctions, territory
445 area, and span ratio, along with an increase in complexity relative to saline-treated
446 mice (Fig. 2E,F; Fig. 5C). These changes suggest a potential shift towards a less
447 reactive phenotype or a different form of reactivity. In the ischemic core, although
448 microglia from MCAO and cortistatin-treated mice looked similar, the treatment still led
449 to distinct microglia with reduced soma size, increased junctions, and decreased span
450 ratio (Fig. 2C,D; Supplementary Fig. 2A,B).

451 To further understand the functional implications of these microglial changes,
452 we analysed the expression of different microglia markers in the ipsilateral hemisphere
453 of saline and cortistatin-treated mice compared to the contralateral hemisphere (Fig.
454 5D). Following MCAO, there was enhanced expression of microglial reactivity markers
455 such as *CD68* and *Trem2*. Remarkably, cortistatin treatment further upregulated the
456 expression of *CD68*, *Trem2*, and *Iba1* compared to the contralateral hemisphere, and
457 compared to MCAO mice (although the latter was not significant) (Fig. 5D).
458 Interestingly, although no changes were observed for the gene expression of CD206
459 between healthy and ischemic brain samples (Supplementary Fig. 3A), there was a
460 significant decrease in *CD163* expression in cortistatin-treated animals, advocating a
461 potential promotion of both anti-inflammatory and increased phagocytic activity of

462 these cells, consistent with the morphological findings and increased microglial density

463 observed in the ischemic core (Fig. 2).

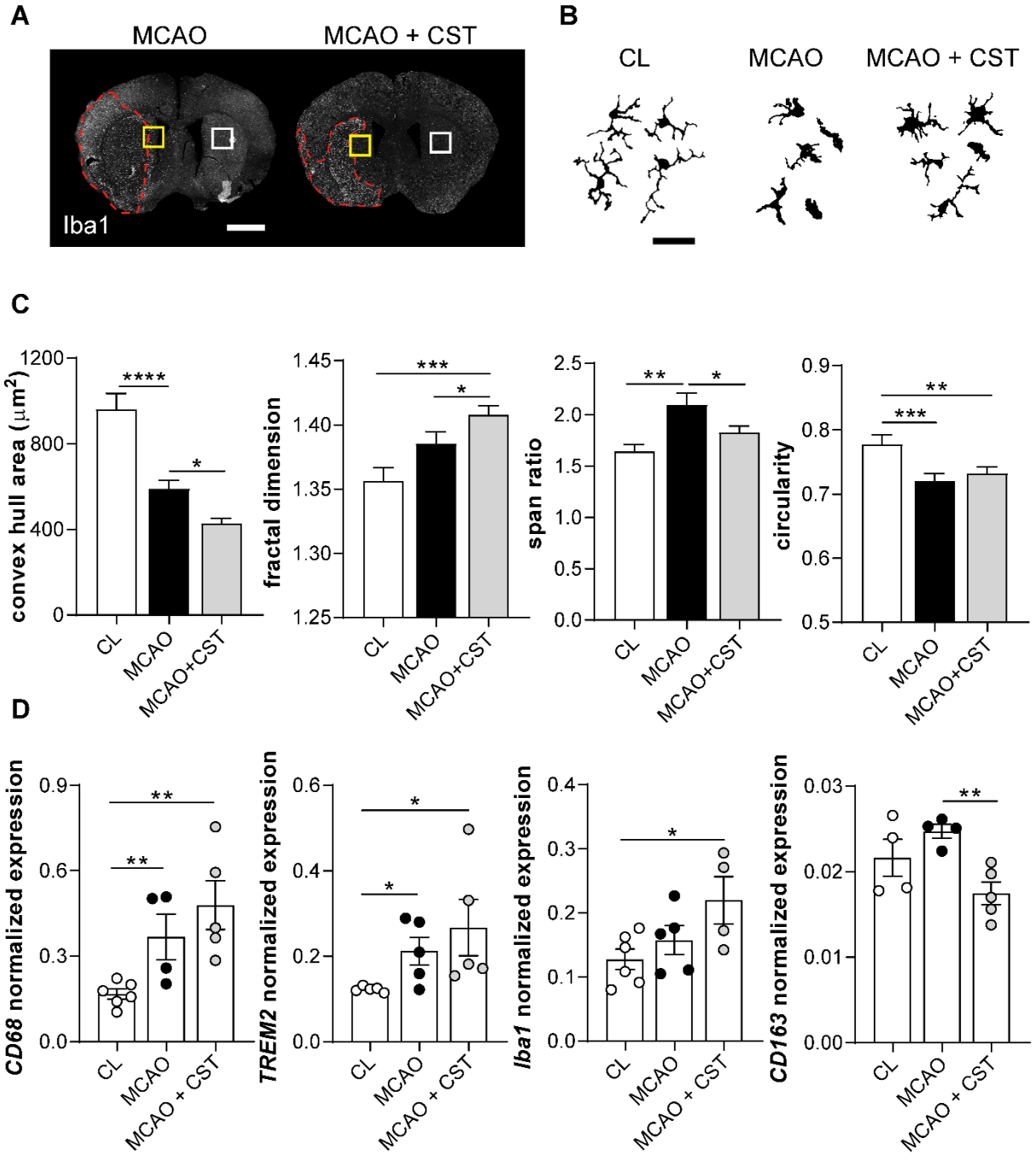

464

465 **Fig. 5. Late administration of cortistatin induces neuroprotective microglia. A.** Brain coronal
466 sections from C57BL/6J mice subjected to MCAO and treated with either saline (MCAO) or cortistatin
467 (144μg/kg) (MCAO+CST) at 24 hours post-reperfusion and sacrificed at 48 hours. Microglia was
468 identified by Iba1 staining. Ischemic core is represented by dashed red lines. Scale bar: 1,500 μm. **B.**
469 Representative binary images of microglia from the ischemic penumbra (yellow square) and the
470 contralateral side (CL) (white square) from the distinct experimental groups. Scale bar: 30 μm. **C.**
471 Morphological parameters of microglia were analysed using Fractal Analysis including convex hull area,

472 fractal dimension/complexity, span ratio, and circularity. n = 15-20 cells/mice; N = 3 mice/group. **D**.
473 Gene expression levels of *CD68, TREM-2, Iba1,* and *CD163* in the contralateral and ipsilateral brain
474 hemispheres of saline and CST-treated MCAO mice were measured by real-time qPCR and normalized
475 to *Rplp0* expression (N=4-6 mice/group). Data are presented as mean ± SEM with dots representing
476 individual mice. **vs.* MCAO, *$p \leq 0.05$, **$p \leq 0.01$, ***$p \leq 0.001$, ****$p \leq 0.0001$. CD68: cluster of
477 differentiation 68, CD163: cluster of differentiation 163, CST: cortistatin, Iba1: ionized calcium-binding
478 adaptor molecule 1, MCAO: middle cerebral artery occlusion, TREM-2: triggering receptor expressed
479 on myeloid cells 2.

480 ### *3.5. Late administration with cortistatin enhances glial scar formation and*
481 ### *astrocyte reactivity*

482 Given the collaborative role of microglia and astrocytes in the context of stroke to limit
483 the damage and prevent its spread [26], we assessed the impact of late cortistatin
484 treatment on the neuroinflammatory response of astrocytes (Fig. 6). Cortistatin
485 treatment resulted in thicker glial scars with astrocytes exhibiting a reduced territory
486 area, complexity index (fractal dimension), and circularity, and an increased span ratio,
487 compared to control MCAO mice (Fig. 6A-C).

488 Along with the fewer junctions, increased area, and enlarged soma shown in
489 Fig.3, these parameters indicate that cortistatin induces a distinct morphotype of
490 hypertrophic reactive astrocytes. To validate our findings, we examined the expression
491 of *GFAP,* a well-known marker of astrocyte reactivity [27]. Following MCAO, both
492 saline and cortistatin-treated mice showed increased *GFAP* expression compared to
493 the contralateral side. However, cortistatin treatment significantly reduced *GFAP*
494 expression relative to MCAO control mice. Thus, these results coupled with the
495 upregulation of neurotrophic and glial factors after cortistatin treatment (Fig. 4,5),
496 suggest that the reactive morphotype exhibited by these astrocytes may exert a role
497 in the establishment of an efficient glial scar and potentially linked to reduced neuronal
498 damage.

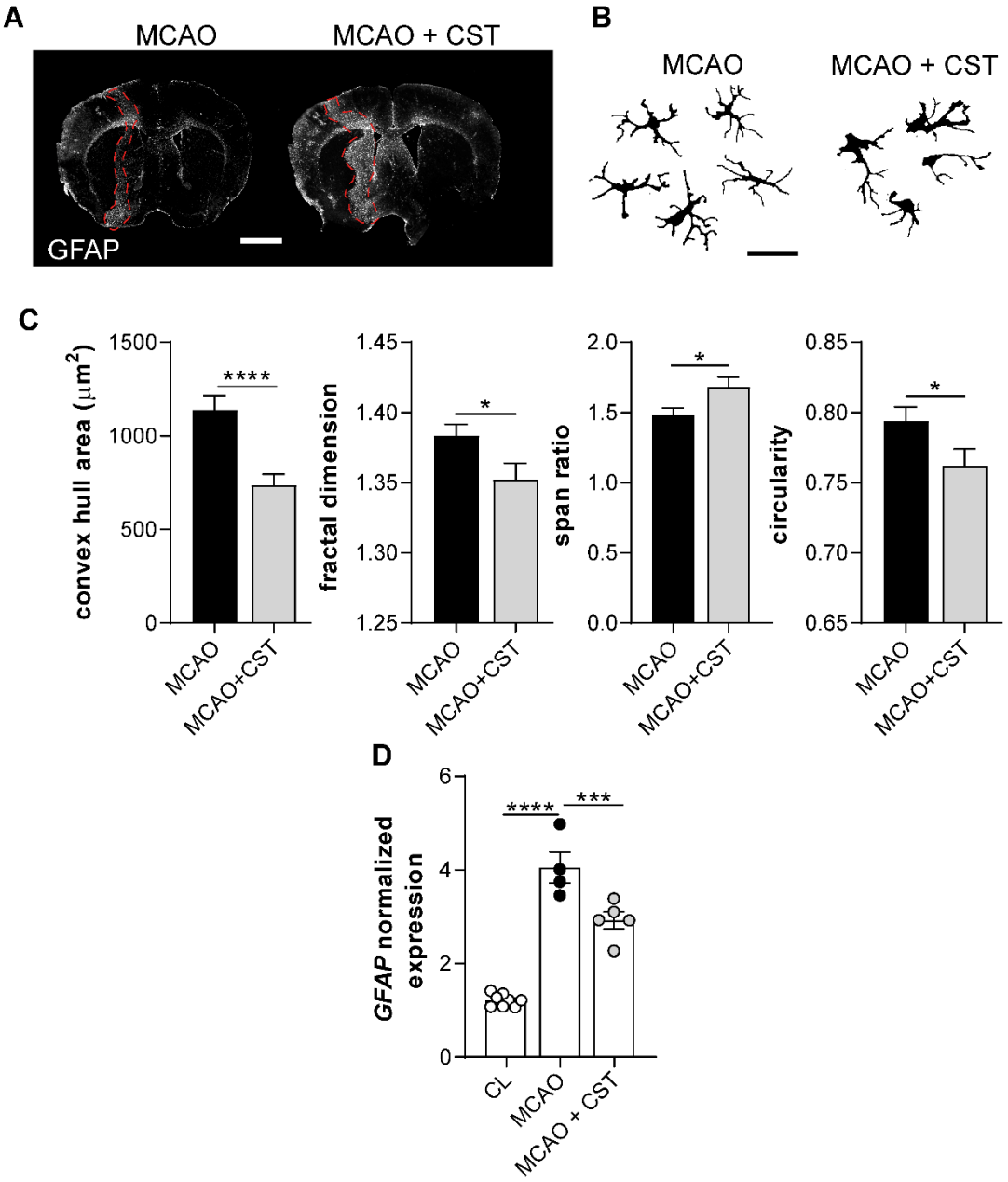

Fig. 6. Late administration of cortistatin promotes protective astrocytic responses in ischemic stroke. A. Brain coronal sections from C57BL/6J mice subjected to MCAO and treated with either saline (MCAO) or cortistatin (144µg/kg) (MCAO+CST) at 24 hours post-reperfusion and sacrificed at 48 hours. Sections were stained with GFAP antibody to identify astrocytes. The astrocyte scar is indicated by dashed red lines. Scale bar: 1,500µm. **B.** Representative binary images of astrocytes from the glial scar were evaluated. Scale bar: 30 µm. **C.** Morphological parameters of astrocytes (convex hull area, fractal dimension/complexity, span ratio, and circularity) were quantified using Fractal Analysis. n = 15-20 cells/mice; N = 3 mice/group. **D**. Gene expression levels of *GFAP* in the contralateral and ipsilateral brain hemispheres of saline and CST-treated MCAO mice were quantified by real-time qPCR and normalized to *Rplp0* expression (N=4-6 mice/group). Data are presented as mean ± SEM with dots representing individual mice. *vs MCAO, *$p \leq 0.05$, ***$p \leq 0.001$, ****$p \leq 0.0001$. CST: cortistatin, GFAP: glial fibrillary acidic protein, MCAO: middle cerebral artery occlusion.

513 Together, these findings highlight cortistatin as a key regulator of glial responses
514 in stroke pathology supporting neuroprotective properties.

515 ### *3.6. Cortistatin protects against BBB breakdown and improves vascular*
516 ### *dynamics after stroke*

517 Stroke is accompanied by the breakdown of the BBB, contributing to neurovascular
518 damage and complications. To thoroughly explore the extent of BBB dysfunction after
519 ischemia in late cortistatin-treated mice, we evaluated IgG leakage. This is one of the
520 key indicators of BBB breakdown, reflecting the extravasation of endogenous blood
521 proteins. In our model, IgG leakage was prominently observed in the ipsilateral
522 hemisphere after stroke, but significantly reduced following cortistatin treatment (Fig.
523 7A,B).

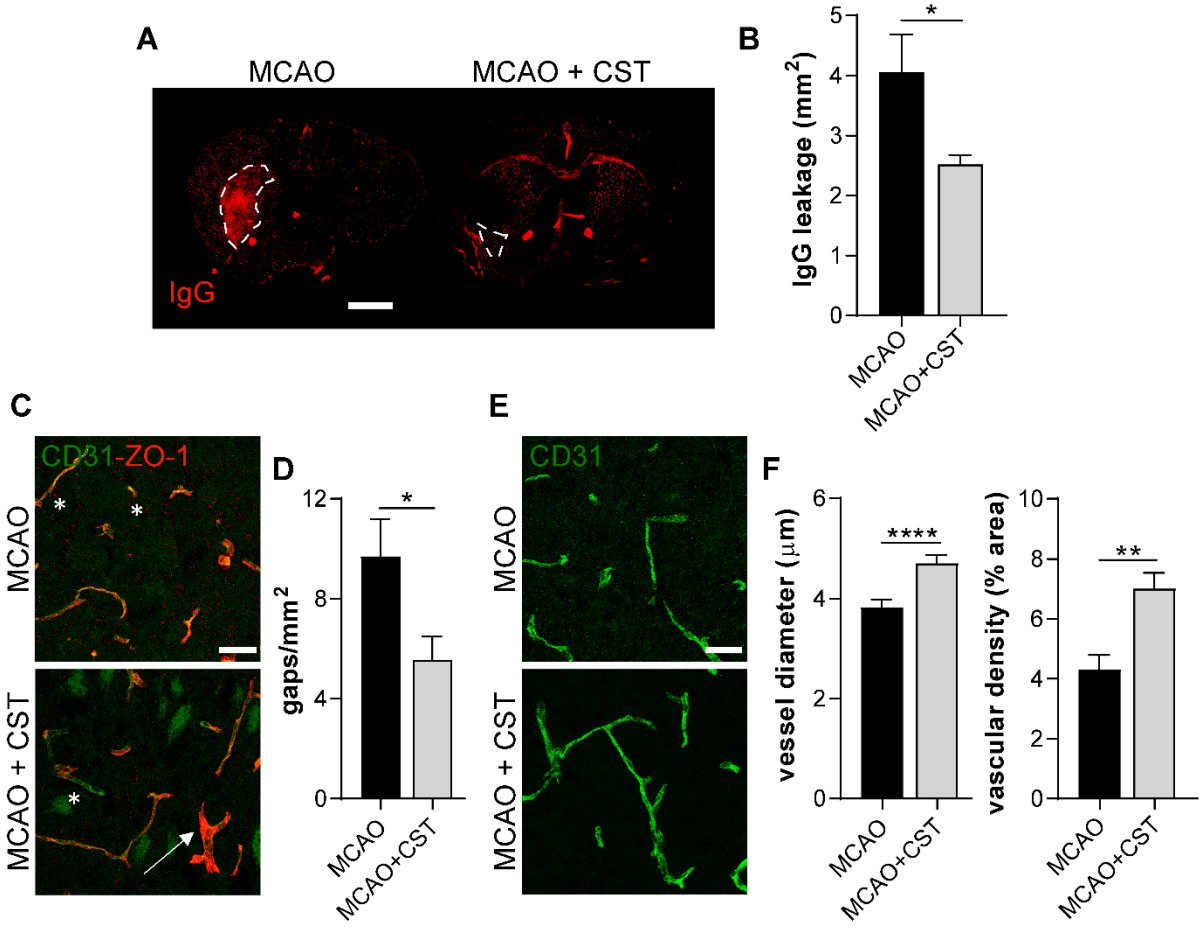

524

525 **Fig. 7. Cortistatin diminishes BBB disruption after stroke. A.** Brain coronal sections from C57BL/6J
526 mice subjected to MCAO and treated with either saline (MCAO) or cortistatin (144µg/kg) (MCAO+CST)
527 at 24 hours post-reperfusion and sacrificed at 48 hours. Sections were stained with a fluorescently-
528 labelled antibody against mouse IgGs. IgG leakage areas are outlined with dashed white lines. Scale
529 bar: 1,500 µm. **B.** IgG^+ area was measured as a quantification of IgG leakage from the blood. N = 4-8
530 mice/group. **C.** Representative images taken in the ipsilateral striatum of mice of the two experimental
531 groups following MCAO and treated with CST, stained with CD31 antibody for brain endothelial cells
532 (BECs, green) and ZO-1 (red) for TJs. ZO-1 gaps are highlighted with an asterisk, while ZO-1 coverage
533 recovery is indicated with arrows. Scale bar: 30 µm. **D.** Quantification of the number of ZO-1 gaps per
534 vessel area. n = 3 ROIs/section/mice; N = 3-5 mice/group. **E.** Representative images of BECs (CD31,
535 green) from the ipsilateral striatum of MCAO or cortistatin-treated mice. Scale bar: 30 µm. **F.** Vessel
536 diameter was manually measured, and vascular density was calculated as the % of positive CD31
537 staining of the total area of the image. n = 10-20 measures/vessel with 5-10 vessels/mice; N = 3-6
538 mice/group. Data are presented as the mean ± SEM. **vs.* MCAO, *$p \leq 0.05$, **$p \leq 0.01$, ****$p \leq 0.0001$.
539 CD31: cluster of differentiation 31, CST: cortistatin, IgG: immunoglobulin G, MCAO: middle cerebral
540 artery occlusion, ZO-1: zonula-occludens 1.

541 After occlusion and reperfusion processes, hypoxic conditions particularly affect
542 brain endothelial cells (BECs), disrupting TJs, leading to increased permeability and
543 contributing to the development of vasogenic edema [28]. We observed that following
544 MCAO, ZO-1 expression in the ischemic core showed disorganized patterns with
545 increased gaps (Fig. 7C,D). Among TJs, disruption of ZO-1 has been extensively
546 documented following stroke [29,30], playing a crucial role in BBB breakdown and
547 subsequent recovery. Conversely, cortistatin treatment mitigated this disorganization,
548 leading to a reduction in the number of ZO-1 gaps, thereby potentially improving TJ
549 integrity (Fig. 7D). We also observed a decrease in the expression of *claudin-1* after
550 MCAO *vs.* the contralateral side, with no alterations after cortistatin treatment
551 (Supplementary Fig. 3B). Additionally, alterations in basement membrane proteins like
552 collagen type I (Col1a2) were observed post-stroke, with cortistatin treatment showing
553 a trend towards increasing *Col1a2* expression levels compared to MCAO alone
554 (Supplementary Fig. 3B). In response to stroke, vascular dynamics undergo significant
555 changes to promote angiogenesis and the modification of the vascular tree [31]. To
556 investigate the importance of this process in stroke recovery, we examined the area
557 occupied by vessels ($CD31^+$) and their diameter in the striatal core (Fig. 7E).

558 Cortistatin treatment enhanced vessel diameter and vascular density in the ischemic
559 striatum compared to saline-treated MCAO mice (Fig. 7F). This enhancement in
560 vascular parameters may facilitate improved reperfusion to the damaged area,
561 supporting post-stroke recovery mechanisms.

562 These findings suggest that cortistatin not only protects against BBB
563 permeability breakdown but also promotes angiogenic and vascular remodelling
564 events that aid in vascular repair and regeneration post-stroke.

565 *3.7. Cortistatin modulates central and peripheral immune responses*
566 *following stroke, reducing brain infiltration and immunodepression*

567 After ischemia-reperfusion injury, the brain undergoes oxidative stress and neuronal
568 death, triggering glial cell activation and the secretion of cytokines and other immune
569 factors. Following MCAO, we observed increased expression of *TNF-α* and *IL-6* in the
570 untreated ischemic brain hemisphere compared to the contralateral side, with no
571 differences in *IL-10* expression. Interestingly, cortistatin treatment significantly
572 elevated *TNF-α* and *IL-10* levels (Fig. 8A). Levels of *IL-1β* showed no significant
573 differences between groups. Additionally, ischemia-induced arginase 1 (*Arg1*)
574 expression, indicative of brain immune infiltration and stroke severity [32,33], was
575 significantly downregulated by cortistatin (Supplementary Fig. 3C). This suggests that
576 cortistatin influences the polarization of immune cells towards a neuroprotective
577 phenotype.

578 Cytokines and DAMPs derived from brain damage can be released into the
579 systemic circulation, getting to lymphoid organs and initiating the peripheral
580 inflammatory response [34]. This triggers the quick adhesion of platelets and
581 leukocytes to the endothelium facilitated by BBB disruption, enabling peripheral

582 immune cells to infiltrate the brain [35]. To explore how cortistatin influences peripheral
583 immune response dynamics, we measured cytokine levels in serum and assessed the
584 infiltration of immune cells into the ischemic core. We observed that in MCAO mice,
585 significant immune infiltration (CD45+ cells) occurred in the ischemic region, which
586 was markedly reduced following cortistatin treatment (Fig. 8B,C). This suggests that
587 cortistatin limits the infiltration of peripheral immune cells into the injured brain,
588 possibly through its effects on BBB integrity.

589 The initial, short-lasting activation of systemic immunity by DAMPs and cytokines
590 released in the bloodstream is swiftly followed by long-lasting immunodepression,
591 characterized by lymphopenia and reduced functional activity of T cells and monocytes
592 among others [36]. In our model, stroke-induced immunodepression was
593 characterized by an oedematous and fibrotic spleen with decreased splenocyte
594 numbers. Cortistatin treatment reversed these effects, significantly increasing the total
595 number of splenocytes and reducing spleen weight after stroke (Fig. 8D). Furthermore,
596 cortistatin treatment restored the reduced stroke-associated serum levels of IL-12 and
597 IL-6 to homeostatic conditions, and increased MCP1 levels, indicating a systemic
598 modulation of inflammatory responses (Fig. 8E).

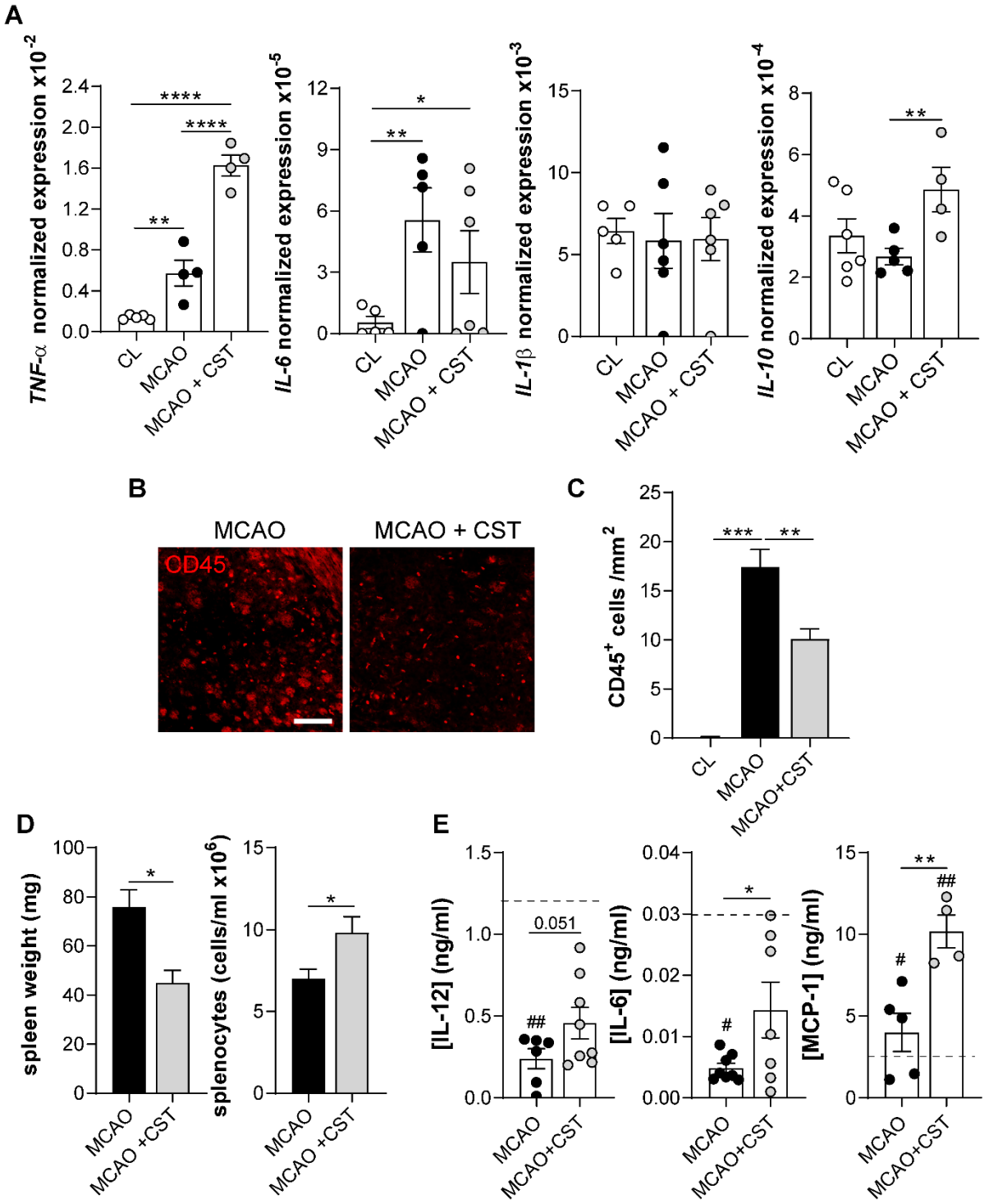

Fig. 8. Cortistatin modulates immune infiltration and peripheral immune response after ischemic stroke. A. Gene expression levels for *TNF-α*, *IL-6*, *IL-1β*, and *IL-10* in the contralateral and ipsilateral brain hemispheres, of saline and CST-treated MCAO mice were quantified using real-time qPCR and normalized to *Rplp0* expression. N = 4-6 independent mice**. B.** Representative brain coronal sections stained with CD45 antibody (red) for leukocytes from C57BL/6J mice subjected to MCAO and treated with saline (MCAO) or cortistatin (MCAO+CST) at 24h post-reperfusion and sacrificed at 48h. Scale bar: 100 µm. **C.** Leukocyte density (number of cells/mm^2) was measured in the striatum and the contralateral side (CL). **D.** Spleen weight and the number of splenocytes/ml were measured. N = 4-8

608 independent mice. **E.** Serum levels of IL-12, IL-6, and MCP-1 (ng/ml) in serum were measured using
609 an ELISA assay. Dashed lines represent cytokine concentrations in healthy mice. N = 3-6 independent
610 mice. Data are the mean ± SEM with dots representing individual mice. ***vs.* MCAO, $^{\#}$*vs.* healthy mice
611 $^{*,\#}p \leq 0.05$, $^{**,\#\#}p \leq 0.01$, $^{***}p \leq 0.001$, $^{****}p \leq 0.0001$. CD45: cluster of differentiation 45, CST: cortistatin,
612 IL-6: interleukin 6, IL-1β: interleukin 1β, IL-10: interleukin 10, IL-12: interleukin 12, MCAO: middle
613 cerebral artery occlusion, MCP-1: Monocyte Chemoattractant Protein-1, TNF-α: tumour necrosis factor-
614 α.

615 In summary, cortistatin administered with an appropriate post-stroke timing
616 exerts multifaceted beneficial effects. It enhances neuroprotective cytokine profiles in
617 the brain, reduces neuronal damage, potentially through the modulation of microglia
618 reactivity and enhancing the formation of the astrocytic scar, regulates BBB integrity
619 preventing immune cell infiltration, and modulates systemic inflammatory responses.
620 Additionally, cortistatin counteracts stroke-induced immunodepression by restoring
621 splenic immune function. These findings underscore the therapeutic potential of
622 cortistatin in stroke by not only protecting neuronal tissue and promoting vascular
623 recovery but also by regulating immune responses to support overall recovery
624 mechanisms.

625 **4. <u>DISCUSSION</u>**

626 The pathogenesis of stroke involves a complex interplay among nervous, circulating,
627 and cerebral immune cells, which can play dual roles influenced by their spatial
628 location, context, and timing [34]. Despite the significance of these factors, many
629 cytoprotective therapeutic approaches have overlooked them, instead focusing on
630 time windows that do not align with the underlying pathophysiology. Typically,
631 interventions target the hyper-acute stage to fit the time range of rtPA, or slightly later,
632 without discriminating the different phases. Therefore, an increased awareness of the
633 intricate spatiotemporal relationships between the nervous, vascular, and immune
634 systems may prove essential for the design of novel therapeutic approaches to
635 improve stroke prognosis.

636 In this context, our findings advocate that the neuropeptide cortistatin, which
637 provides a crucial link between the CNS and the immune system, could be a promising
638 therapeutic agent, positively influencing different aspects of stroke pathophysiology
639 when administered at appropriate stages. Surprisingly, when cortistatin was given
640 immediately after blood flow restoration, it worsened neuronal damage, motor
641 performance, and neurological scores. The decreased microglial density with
642 increased ameboid-like microglia in the core and the hyper-ramified microglial
643 phenotype in the penumbra might be related to the potent immunomodulatory effects
644 of cortistatin. The neuropeptide administered shortly after reperfusion may blunt the
645 initial endogenous response of microglia that tries to limit the ischemic damage.
646 Cortistatin may have prompted microglia to respond with an initially protective but later
647 excessively reactive phenotype. Furthermore, the immediate cortistatin treatment
648 appeared to hinder the initial astrocytic response, as evidenced by the disorganized
649 astrocytic scar, preventing the formation of well-defined astrocytic borders, and
650 potentially facilitating the expansion of neuronal damage.

651 Conversely, treatment with cortistatin at a slightly later stage (4h + 24h) did not
652 reduce infarct volume or improve neurological outcomes. This treatment did not affect
653 microglia density or morphotype in the core but induced a hyper-ramified microglia
654 phenotype in the perilesional area. The early treatment with cortistatin enhanced the
655 formation of the glial scar, possibly because it coincided with the initiation of the
656 astrocytic response [37], modulating astrocytes differently than at the 0-hour time-point
657 treatment. These findings underscore the critical importance of timing in therapeutic
658 intervention, as even a few hours can have a strong effect on the response to the
659 treatment. Indeed, late cortistatin administration (24h) appeared to lead to reduced
660 neuronal lesions and improved outcomes.

661 The lack of protection observed with the immediate administration might seem
662 contradictory to the beneficial effect shown at 24h and to the reported beneficial effects
663 of cortistatin administration in other neurodegenerative/neuroinflammatory disorders
664 [8,11,12]. However, the latter studies involved cortistatin injection at later stages of the
665 disorder (*i.e.,* when the injury is well-established), while in our investigation the
666 immediate administration coincided with the initial stages of injury. This suggests that
667 the observed harmful effects on outcome are not likely due to cortistatin being
668 neurotoxic but rather that when administered immediately or early after stroke,
669 cortistatin interferes with the initial local neuroinflammatory response that is essential
670 for containing the damage and removing debris and dead cells (*i.e.,* glial scar
671 formation and microglia response, respectively), thereby leading to detrimental
672 neurological outcome. The timing of cortistatin administration therefore appears vital
673 to the subsequent progression of brain healing processes. Indeed, blocking or
674 modifying the important early response leads to adverse outcomes in other disorders.
675 For instance, Szalay *et al.* demonstrated that depletion of microglia resulted in a
676 significant enhancement of lesion size, which was reversed by microglial repopulation
677 [38]. These findings may also explain the lack of clinical success reported with some
678 anti-inflammatory/immunomodulatory drugs administered at too early phases [3].
679 Collectively, these data underscore the fundamental role of the inflammatory response
680 in the regenerative process after stroke and suggest that these mechanisms should
681 not be completely halted. Instead, modulating the inflammatory response, rather than
682 attempting to stop it entirely, seems to be a more effective approach.

683 Given these first results, we focused on a deeper investigation of the effect of
684 cortistatin administration at the late stage. This approach, besides providing more
685 flexibility in treatment application, also enables concurrent administration with other

686 therapies such as rtPA. First, we confirmed the reduced striatal lesion size following
687 late (24h) cortistatin treatment based on CV and MAP-2 immunodetection. Notably,
688 MAP-2 provides a better insight into the first phases of neuronal death, even if the
689 process is not yet concluded [39]. This indicated that cortistatin efficiently targeted
690 neuronal death, protecting neuronal bodies, also evidenced by the increased
691 expression of neuroprotective factors such as *BDNF* or *GDNF*. GDNF is important for
692 the maintenance of dopaminergic neurons and their protection against injury [40],
693 while BDNF protects neurons from ischemia-reperfusion-induced apoptosis [41]. The
694 neuroprotective role of cortistatin conforms with previous research, where we and
695 others demonstrated that treatment with the neuropeptide protected neurons from
696 distinct insults *in vivo* and *in vitro* [12,42]. However, it is not clear yet the underlying
697 mechanisms (*i.e.,* inhibition of apoptosis, neuronal degeneration, or oxidative
698 damage). Moreover, we can hypothesize that cortistatin might also exert an indirect
699 beneficial effect on neurons by regulating the responses of glial cells.

700 For decades, ischemic stroke research has primarily focused on rescuing
701 neurons in the penumbra region to prevent the expansion of the infarct core. However,
702 given that excitotoxicity, oxidative stress, neuroinflammation, or peripheral immune
703 response contribute to secondary neuronal cell death [43] and that focusing solely on
704 neuronal death is oversimplistic [44], this study aimed to explore the impact of
705 cortistatin on the stroke-induced neuroinflammatory response. Microglia are the initial
706 responders to ischemic damage, swiftly undergoing dynamic morphological and
707 molecular changes in the infarct core and the peri-infarct zone [45]. Importantly,
708 microglia undergo multiple alterations after injury (*e.g.,* degree and length of
709 branching, branch configuration, shape and soma size, cell territory, receptor
710 distribution, or cytoskeletal rearrangement), that go beyond the oversimplified

711 paradigm of M1/M2 or the traditional morphological characterization categorizing
712 microglia as either ramified (homeostatic) or reactive (short processes) [46]. Our
713 findings showed an increased number of microglial cells in the ischemic core after late
714 treatment with cortistatin. Moreover, elevated expression of markers related to
715 phagocytosis (*i.e., CD68, Trem2*) was also found in the ipsilateral hemisphere of
716 cortistatin-treated mice, consistent with the enhanced phagocytic phenotype and
717 neuroprotective microglial function reported in early stages of stroke [47,48]. Since
718 cortistatin significantly reduced brain lesions, these findings suggest an enhanced
719 phagocytosis of dead neurons by the microglia from cortistatin-treated mice. Indeed,
720 previous studies have demonstrated that endogenous cortistatin is essential for
721 phagocytosis in physiological and demyelinating environments [49]. However,
722 hyperreactive microglia over time can engulf live or stressed neurons, resulting in
723 worsened neurological deficits [50], emphasizing the need to maintain a careful
724 balance to ameliorate stroke prognosis. Microglia in the ischemic core exhibited
725 reduced soma size and a larger number of junctions following cortistatin treatment,
726 suggesting a shift to a more protective phenotype, diverging from the ameboid-like
727 shape phenotype observed in control mice. While most microglia are engaged in
728 engulfing dead neurons and secreting neurotrophic factors in the ischemic core, those
729 in the peri-infarct area exhibit a different phenotypic polarization, influenced by
730 surrounding factors [51,52]. Cortistatin treatment shifted peri-infarct microglia to a
731 distinct reactive phenotype characterized by a reduced territory and soma but
732 increased complexity. Moreover, elevated levels of *TNF-α*, *IL-10*, and neuroprotective
733 factors such as *BDNF* or *GDNF* were detected. These results suggest a potential
734 transformation to a distinct subtype of protective/reactive microglia, capable of
735 phagocytosing cellular debris while aiding brain regeneration [53]. This is confirmed

736 by previous findings in other neuroinflammatory models (*i.e.,* multiple sclerosis,
737 Parkinson's disease, and sepsis) [8,12,54], where cortistatin-modulated microglia
738 markedly correlated with a better disease prognosis. Conversely, we observed a
739 decreased expression of the scavenger receptor *CD163*, involved in the clearance of
740 haemoglobin [55]. Interestingly, this factor is upregulated in patients with intracerebral
741 haemorrhage and edema development [56], suggesting a potential reduction of these
742 events following cortistatin treatment. Overall, the unique combination of phagocytic
743 function, inflammatory cytokines, and neurotrophic/neuroprotective factors secreted
744 by these cells may play a crucial role in promoting neuron survival and modulating
745 other neuroinflammatory responses. Although many questions remain unanswered
746 regarding the transitions between the different subsets of glial cells and the key
747 molecular cues that drive these transitions [23], our study indicates that cortistatin may
748 play an important role in this context. However, acknowledging the limitations of our
749 study, we could not determine the exact molecular and functional morphotype of these
750 cells in terms of spatial and temporal dynamics, since the gene expression analysis
751 could not discriminate between different brain areas within the same hemisphere,
752 different cell populations, or different cell subsets. Additionally, we cannot dismiss the
753 fact that more than one cell type produces the same factor, further complicating the
754 interpretation of our results. To address these limitations, further studies are needed
755 to explore the exact mechanisms through which cortistatin-modulated microglia exert
756 this immunomodulatory role.

757 Astrocytes also play essential roles in stroke, modulating the
758 neuroinflammatory response, protecting neurons by releasing neuroprotective factors,
759 forming barriers to limit damage, and promoting brain repair [57]. Although the
760 molecular and cellular mechanisms that underlie the formation of the glial scar and

761 astrocyte reactivity are not completely understood, they likely involve a complex and
762 balanced interplay of molecular signals that can simultaneously boost phagocytosis
763 and debris clearance, which would be essential for the protection and conservation of
764 the still-healthy tissue [37,57,58]. Similar to microglia, an A1/A2 paradigm for astrocyte
765 morphology and function has been proposed [59,60]. However, the spatiotemporal
766 heterogeneity of reactive astrocytes has demonstrated that this classification is too
767 simple, so additional parameters should be considered [61]. Our study revealed that
768 cortistatin-treated mice exhibited a well-organized and thicker glial scar than control
769 mice. This was accompanied by an increased expression of neurotrophins, which have
770 been described to be involved in synaptic plasticity and neuronal growth regulation
771 that tend to decrease in pathological CNS processes [62]. Thus, cortistatin promotes
772 a distinct reactive phenotype that supports tissue repair and neuroprotection. An
773 effective glial scar is critical as defective scar formation has been associated with
774 larger lesions, demyelination, and reduced neuronal survival and functional recovery
775 [37,58,63]. However, an excessive glial scar can be detrimental by exacerbating
776 inflammation and interfering with synaptic and axonal growth [37]. The observed
777 localization and cortistatin-dependent timing of astrocyte activation in our study
778 indicate a controlled and neuroprotective response to limit damage following cortistatin
779 treatment.

780 In addition, BBB integrity is needed for better stroke outcomes [64]. The
781 traditional classification of BBB changes during stroke progression is restricted to
782 “opening” or “closing” (*i.e.,* "bad" or " good”) making this dichotomy outdated [65].
783 Instead, BBB permeability follows a sequence across different phases (*i.e.,*
784 hyperacute, acute, subacute, and chronic phases), each of them characterized by
785 distinct biological events [65]. Our study specifically focused on the acute phase in

786 which BBB permeability peaks, facilitating neuroinflammation progression and
787 exacerbating injury [66]. Our findings demonstrated that cortistatin treatment helped
788 preserve BBB integrity by reducing endothelial dysfunction and maintaining tight
789 junctions, as evidenced by the decreased IgG leakage and reduced number of ZO-1
790 gaps. These results align with previous studies showing that cortistatin protects the
791 BBB in models of mild neuroinflammation and *in vitr*o models of BBB disruption [13].
792 Interestingly, the lack of changes in claudin-1 and claudin-5 gene expression suggests
793 that TJ alterations may occur at the protein localization level rather than at the gene
794 expression level [67–69]. Indeed, cortistatin has demonstrated a role in modulating
795 protein levels, cellular redistribution, and functional organization of BBB proteins such
796 as ZO-1, claudin-1, claudin-5, and VE-cadherin without significantly affecting their
797 transcript levels [13].

798 Finally, it is important to acknowledge that stroke is a complex, organism-wide
799 process that not only targets the brain but also peripheral tissues. Shortly after the
800 interruption of the CBF and subsequent hypoxia, ECs express selectins in response
801 to oxidative damage, quickly engaging circulating innate immune cells, and triggering
802 a rapid pro-inflammatory response in the periphery [2]. The breakdown of various
803 components of the BBB enables the extravasation of these cells, with different
804 cadences and at variable times. In general, a well-regulated inflammatory response is
805 inherently self-limiting, facilitating the repair, turnover, and tissue adaptation, and
806 prioritizing processes that restore homeostasis over those that are harmful [70,71].
807 The immunomodulatory effects of cortistatin were evident as it reduced immune cell
808 infiltration into the brain and modulated systemic immune responses, consistent with
809 its effects observed in other neuroinflammatory models [8,13]. Specifically, cortistatin
810 treatment modulated the expression of typically pro-inflammatory cytokines (*e.g.,* IL-

811 6, TNF-α, IL-12) in the brain. These cytokines exert biphasic or even polyphasic roles
812 in ischemic stroke, and depending on the timing, spatial location, and severity of the
813 injury, they can play vital roles in repair processes or have detrimental effects. For
814 example, it has been shown that the deletion of IL-6 in MCAO mice does not confer
815 protection against cerebral ischemia [70]. Indeed, IL-6 serves as a neurotrophic factor,
816 improving functional outcomes, reducing stroke volume in mice [72], and promoting
817 post-stroke angiogenesis [73]. Similarly, numerous studies have reported a
818 neuroprotective role of TNF-α in reducing the production of nitric oxide and free
819 radicals, maintaining neuronal calcium homeostasis, and inducing the synthesis of
820 neurotrophic factors [74]. Hence, these data, along with the increased levels of anti-
821 inflammatory factors (*i.e.,* IL-10), the reduced number of infiltrating cells, and the
822 decreased neuronal damage suggest that the elevated inflammatory factors observed
823 after the treatment with the neuropeptide might be crucial for developing an
824 appropriate response to the acute damage and subsequent resolution rather than
825 playing a detrimental role. This underscores the complexity of the immune response
826 in stroke and, again, the importance of the timing of therapeutic intervention.

827 This initial activation of systemic immunity is quickly succeeded by a prolonged
828 state of immunodepression, which enhances the susceptibility to infection or other
829 pathologies [36]. Depression of the immune system not only occurs in patients with
830 ischemic stroke but also in other acute CNS injuries such as cerebral haemorrhage,
831 traumatic brain injury, or spinal cord trauma (reviewed in [36]). In this sense, the
832 observed potent immunomodulatory role of cortistatin, especially regarding spleen
833 function and cytokine recovery to homeostatic levels, is consistent with other studies
834 [8,75,76]. Interestingly, we found elevated levels of MCP-1 after cortistatin treatment.
835 Although this factor is systemically upregulated in stroke patients and is known to

836 promote leukocyte chemotaxis, some reports also demonstrate that MCP-1 is crucial
837 for recruiting neural stem cells after stroke, which is necessary for better neurological
838 outcomes [77]. Along these lines, we also found that cortistatin reduced the elevated
839 levels of *Arg1*, which is consistently upregulated in stroke patients [32], and known to
840 induce lymphopenia in a murine model of stroke [78]. Indeed, Arg1 inhibition
841 ameliorates stroke outcomes [79] and it is already been used in clinical trials in patients
842 with coronary artery disease who have suffered from ischemia-reperfusion [80].

843 In summary, with timely administration, the neuroimmune-modulatory role of
844 cortistatin in stroke extends beyond its direct neuroprotective effects on brain damage,
845 glial responses, and BBB modulation, to include the regulation of systemic immune
846 responses and to positively affect detrimental behavioural and functional outcomes.
847 This multifaceted mechanism of action offers several advantages over therapies
848 targeting single aspects of stroke pathophysiology. Furthermore, the intriguing
849 possibility that this neuropeptide has a role in the main players in this condition (such
850 as neurons, astrocytes, microglia, BECs, pericytes, or immune cells) could confer an
851 advantage over other potential therapies. Notably, the physiological nature—and thus
852 intrinsically non-toxic properties—of this neuropeptide provide assurances of its
853 potential use. In fact, it has been successfully used at clinical levels, both systemically
854 and locally, demonstrating its therapeutic efficacy in patients with acromegaly,
855 prolactinoma [81], and Cushing's disease [82]. Being beyond the scope of this work,
856 further research should consider sex as an independent variable that must be
857 addressed to properly interpret the beneficial action of cortistatin. Future studies
858 should also focus on extending the investigation of the spatiotemporal dynamics of
859 cortistatin action, the molecular pathways involved, and its effects on other cell types
860 within the CNS and the peripheral immune system.

861 **CONCLUSION**

862 Our data underscore the importance of comprehending the spatio-temporal dynamics
863 of ischemic stroke when devising therapeutic interventions to optimize stroke
864 outcomes. The findings indicating that a too-potent anti-inflammatory effect of the
865 neuropeptide is deleterious when given immediately after stroke, emphasize the need
866 to shift therapeutic goals from halting specific processes to modulating and balancing
867 them, thereby mitigating possible chronic adverse responses. We showed that
868 cortistatin administered at later stages appears to be a very promising candidate drug
869 to enhance recovery after stroke, alone or in combination with other treatments, mainly
870 targeting the outcome of patients that underwent recanalization or spontaneous
871 reperfusion. Our study further highlighted the multifaceted roles of cortistatin in stroke
872 pathophysiology, emphasizing its potential as a therapeutic agent. Its capacity to
873 simultaneously act on various pathological features, such as neuronal damage, glial
874 over-reaction, astrocytic scar formation, and BBB breakdown with an overall
875 amelioration of the neurological outcome, offers significant advantage over
876 interventions targeting single aspects of this condition. Moreover, cortistatin stands as
877 a key factor regulating the complex interplay between the CNS and the immune
878 system, modulating exacerbated molecular and cellular responses from both systems
879 that may affect the brain's recovery processes. Finally, the valuable insights gained
880 from this research have the potential to advance the development of novel therapeutic
881 approaches, not only targeting stroke pathology but also other CNS disorders linked
882 to glial over-reactivity, BBB disruption, or dysfunctional CNS-immune system
883 interactions. Future research should continue to explore the complex interplay
884 between this neuropeptide, its receptors, and the multitarget effects in stroke to
885 develop more effective therapeutic strategies.

886 **ACKNOWLEDGEMENTS**

887 The authors would like to thank the Animal Care Unit and Microscopy Service Unit
888 staff from IPBLN for the technical support.

889 **FUNDING**

890 This work was supported by the Spanish Ministry of Science and Innovation
891 (MCIN)/AEI/ 10.13039/501100011033 and by "ERDF A way of making Europe" grants:
892 SAF2017-85602-R and PID2020-119638RB-I00 (to E.G-R.), by the Swiss Science
893 Foundation grant N°310030_212233 and Biaggi Foundation grant (to L.H), and by
894 FPU-program FPU17/02616 and EMBO-STFL8942 (to J.C-G.), FPI-program
895 PRE2018-084824 (to I.S-M.) and PRE2021-100172 (to P.V-R.).

896 **CONTRIBUTIONS**

897 E.G-R conceived, designed and supervised the whole study. J.C-G and E.G-R
898 outlined the experiments and analysed all the data. J.C-G, L.B, P.V-R, I.S-M, and I.F-
899 L performed the experiments. J.C-G, L.B, M.P, P.H-C, L.H, and E.G-R interpreted the
900 data, and discussed the results. J.C-G and E.G-R wrote and drafted the manuscript.
901 J.C-G, E.G-R, L.B, M.P, and L.H revised the manuscript. All authors have read and
902 agreed to the published version of the manuscript.

903 **ETHICS DECLARATION**

904 **Ethical approval**

905 All procedures were approved by the Animal Care and Use Board and the Ethical
906 Committee of the Spanish National Research Council (Spain), and the Vaud Cantonal
907 Veterinary Office (Switzerland). All experimental protocols adhered to the guidelines
908 specified in Directive 2010/63/EU of the European Parliament and the corresponding
909 Swiss regulations regarding animal protection for scientific purposes.

910 **Competing interests**

911 The authors declare no competing interests.

912 **DATA AVAILABILITY**

913 All data used or analysed will be made available upon reasonable request to the

914 corresponding author.

915 **ABBREVIATIONS**

916 Arg1: arginase 1
917 BBB: blood-brain barrier
918 BDNF: brain-derived neurotrophic factor
919 BECs: brain endothelial cells
920 BL: baseline
921 CBF: cerebral blood flow
922 Cl: claudin
923 CD: cluster of differentiation
924 CL: contralateral
925 CNS: central nervous system
926 CST: cortistatin
927 CV: cresyl violet
928 DAMPs: danger-associated molecular pattern molecules
929 GDNF: glial cell-derived neurotrophic factor
930 GFAP: glial fibrillary acidic protein
931 Iba1: ionized calcium-binding adaptor molecule 1
932 IgG: immunoglobulin G
933 IL: Interleukin
934 MAP-2: microtubule-associated protein 2
935 MBP: myelin basic protein
936 MCAO: middle cerebral artery occlusion
937 MCP-1: monocyte chemoattractant protein-1
938 PFA: paraformaldehyde
939 Rplp0: ribosomal protein lateral stalk subunit P0
940 rtPA: recombinant tissue plasminogen activator
941 TJ: tight-junctions

TNF: tumour necrosis factor- α

Trem2: triggering receptor expressed on myeloid cells 2

ZO-1: zonula occludens 1

BIBLIOGRAPHY

1. Lapchak PA, Yang G-Y, editors. Translational Research in Stroke [Internet]. Singapore: Springer Singapore; 2017. Available from: http://link.springer.com/10.1007/978-981-10-5804-2

2. Campbell BCV, De Silva DA, Macleod MR, Coutts SB, Schwamm LH, Davis SM, et al. Ischaemic stroke. Nat Rev Dis Primers. 2019;5:1–22.

3. Drieu A, Levard D, Vivien D, Rubio M. Anti-inflammatory treatments for stroke: from bench to bedside. Ther Adv Neurol Disord. 2018;11:1756286418789854.

4. de Lecea L, Criado JR, Prospero-Garcia O, Gautvik KM, Schweitzer P, Danielson PE, et al. A cortical neuropeptide with neuronal depressant and sleep-modulating properties. Nature. 1996;381:242–5.

5. Delgado M, Gonzalez-Rey E. Role of Cortistatin in the Stressed Immune System. In: Savino W, Guaraldi F, editors. Frontiers of Hormone Research. S. Karger AG; 2017. p. 110–20. Available from: https://www.karger.com/Article/FullText/452910

6. Córdoba-Chacón J, Gahete MD, Pozo-Salas AI, Martínez-Fuentes AJ, de Lecea L, Gracia-Navarro F, et al. Cortistatin is not a somatostatin analogue but stimulates prolactin release and inhibits GH and ACTH in a gender-dependent fashion: potential role of ghrelin. Endocrinology. 2011;152:4800–12.

7. Deghenghi R, Papotti M, Ghigo E, Muccioli G. Cortistatin, but not somatostatin, binds to growth hormone secretagogue (GHS) receptors of human pituitary gland. J Endocrinol Invest. 2001;24:RC1-3.

8. Souza-Moreira L, Morell M, Delgado-Maroto V, Pedreño M, Martinez-Escudero L, Caro M, et al. Paradoxical Effect of Cortistatin Treatment and Its Deficiency on Experimental Autoimmune Encephalomyelitis. J Immunol. 2013;191:2144–54.

9. Chiu C-T, Wen L-L, Pao H-P, Wang J-Y. Cortistatin Is Induced in Brain Tissue and Exerts Neuroprotection in a Rat Model of Bacterial Meningoencephalitis. J Infect Dis. 2011;204:1563–72.

10. Braun H, Schulz S, Becker A, Schröder H, Höllt V. Protective effects of cortistatin (CST-14) against kainate-induced neurotoxicity in rat brain. Brain Res. 1998;803:54–60.

11. Falo CP, Benitez R, Caro M, Morell M, Forte-Lago I, Hernandez-Cortes P, et al. The Neuropeptide Cortistatin Alleviates Neuropathic Pain in Experimental Models of Peripheral Nerve Injury. Pharmaceutics. 2021;13:947.

12. Serrano-Martínez I, Pedreño M, Castillo-González J, Ferraz-de-Paula V, Vargas-Rodríguez P, Forte-Lago I, et al. Cortistatin as a Novel Multimodal Therapy for the Treatment of Parkinson's Disease. Int J Mol Sci. 2024;25:694.

13. Castillo-González J, Ruiz JL, Serrano-Martínez I, Forte-Lago I, Ubago-Rodriguez A, Caro M, et al. Cortistatin deficiency reveals a dysfunctional brain endothelium with impaired gene pathways, exacerbated immune activation, and disrupted barrier integrity. J Neuroinflammation. 2023;20:226.

14. Buscemi L, Price M, Bezzi P, Hirt L. Spatio-temporal overview of neuroinflammation in an experimental mouse stroke model. Sci Rep. 2019;9:507.

15. Buscemi L, Price M, Castillo-González J, Chatton J-Y, Hirt L. Lactate Neuroprotection against Transient Ischemic Brain Injury in Mice Appears Independent of HCAR1 Activation. Metabolites. 2022;12:465.

16. Lee S, Hong Y, Park S, Lee S-R, Chang K-T, Hong Y. Comparison of surgical methods of transient middle cerebral artery occlusion between rats and mice. J Vet Med Sci. 2014;76:1555–61.

17. Balkaya M, Kröber JM, Rex A, Endres M. Assessing post-stroke behavior in mouse models of focal ischemia. J Cereb Blood Flow Metab. 2013;33:330–8.

18. Fernández-Arjona M del M, Grondona JM, Granados-Durán P, Fernández-Llebrez P, López-Ávalos MD. Microglia Morphological Categorization in a Rat Model of Neuroinflammation by Hierarchical Cluster and Principal Components Analysis. Front Cell Neurosci. 2017;11:235.

19. Young K, Morrison H. Quantifying Microglia Morphology from Photomicrographs of Immunohistochemistry Prepared Tissue Using ImageJ. J Vis Exp. 2018;57648.

20. Schindelin J, Arganda-Carreras I, Frise E, Kaynig V, Longair M, Pietzsch T, et al. Fiji: an open-source platform for biological-image analysis. Nat Methods. 2012;9:676–82.

21. Rousselet E, Kriz J, Seidah NG. Mouse Model of Intraluminal MCAO: Cerebral Infarct Evaluation by Cresyl Violet Staining. J Vis Exp. 2012;e4038.

22. Türeyen K, Vemuganti R, Sailor KA, Dempsey RJ. Infarct volume quantification in mouse focal cerebral ischemia: a comparison of triphenyltetrazolium chloride and cresyl violet staining techniques. J Neurosci Methods. 2004;139:203–7.

23. Qin C, Zhou L-Q, Ma X-T, Hu Z-W, Yang S, Chen M, et al. Dual Functions of Microglia in Ischemic Stroke. Neurosci Bull. 2019;35:921–33.

24. Karperien A, Ahammer H, Jelinek H. Quantitating the subtleties of microglial morphology with fractal analysis. Front Cell Neurosci 2013;7.

25. Peng L, Hu G, Yao Q, Wu J, He Z, Law BY-K, et al. Microglia autophagy in ischemic stroke: A double-edged sword. Front Immunol. 2022;13.

26. Linnerbauer M, Rothhammer V. Protective Functions of Reactive Astrocytes Following Central Nervous System Insult. Front Immunol. 2020;11.

27. Jurga AM, Paleczna M, Kadluczka J, Kuter KZ. Beyond the GFAP-Astrocyte Protein Markers in the Brain. Biomolecules. 2021;11:1361.

28. Thal S, Luh C, Schaible E-V, Timaru-Kast R, Hedrich J, Luhmann H, et al. Volatile Anesthetics Influence Blood-Brain Barrier Integrity by Modulation of Tight Junction Protein Expression in Traumatic Brain Injury. PloS one. 2012;7:e50752.

29. Abdullahi W, Tripathi D, Ronaldson PT. Blood-brain barrier dysfunction in ischemic stroke: targeting tight junctions and transporters for vascular protection. Am J Physiol Cell Physiol. 2018;315:C343–56.

30. Jiao H, Wang Z, Liu Y, Wang P, Xue Y. Specific Role of Tight Junction Proteins Claudin-5, Occludin, and ZO-1 of the Blood–Brain Barrier in a Focal Cerebral Ischemic Insult. J Mol Neurosci. 2011;44:130–9.

31. Rust R. Insights into the dual role of angiogenesis following stroke. J Cereb Blood Flow Metab. 2020;40:1167–71.

32. Petrone AB, O'Connell GC, Regier MD, Chantler PD, Simpkins JW, Barr TL. The Role of Arginase 1 in Post-Stroke Immunosuppression and Ischemic Stroke Severity. Transl Stroke Res. 2016;7:103–10.

33. Li T, Zhao J, Gao H. Depletion of Arg1-Positive Microglia/Macrophages Exacerbates Cerebral Ischemic Damage by Facilitating the Inflammatory Response. Int J Mol Sci. 2022;23:13055.

34. Iadecola C, Anrather J. The immunology of stroke: from mechanisms to translation. Nat Med. 2011;17:796–808.

35. Iadecola C, Buckwalter MS, Anrather J. Immune responses to stroke: mechanisms, modulation, and therapeutic potential. J Clin Invest. 2020;130:2777–88.

36. Westendorp WF, Dames C, Nederkoorn PJ, Meisel A. Immunodepression, Infections, and Functional Outcome in Ischemic Stroke. Stroke. 2022;53:1438–48.

37. Wanner IB, Anderson MA, Song B, Levine J, Fernandez A, Gray-Thompson Z, et al. Glial Scar Borders Are Formed by Newly Proliferated, Elongated Astrocytes That Interact to Corral Inflammatory and Fibrotic Cells via STAT3-Dependent Mechanisms after Spinal Cord Injury. J Neurosci. 2013;33:12870–86.

38. Szalay G, Martinecz B, Lénárt N, Környei Z, Orsolits B, Judák L, et al. Microglia protect against brain injury and their selective elimination dysregulates neuronal network activity after stroke. Nat Commun. 2016;7:11499.

39. Kharlamov A, LaVerde GC, Nemoto EM, Jungreis CA, Yushmanov VE, Jones SC, et al. MAP2 immunostaining in thick sections for early ischemic stroke infarct volume in non-human primate brain. J Neurosci Methods. 2009;182:205–10.

40. Duarte EP, Curcio M, Canzoniero LM, Duarte CB. Neuroprotection by GDNF in the ischemic brain. Growth Factors. 2012;30:242–57.

41. Endres M, Fan G, Hirt L, Fujii M, Matsushita K, Liu X, et al. Ischemic brain damage in mice after selectively modifying BDNF or NT4 gene expression. J Cereb Blood Flow Metab. 2000;20:139–44.

42. Rubio A, Sánchez-Mut JV, García E, Velasquez ZD, Oliver J, Esteller M, et al. Epigenetic control of somatostatin and cortistatin expression by β amyloid peptide. J Neurosci Res. 2012;90:13–20.

43. Fan P, Zhang, L., He, Z., Shao, P., Ding, L., Wang, G., Niu, W., et al. Reduced Severity of Outcome of Recurrent Ipsilateral Transient Cerebral Ischemia Compared with Contralateral Transient Cerebral Ischemia in Rats. J Stroke Cerebrovasc Dis. 2017;26, 2915–2925.

44. Ermine CM, Bivard A, Parsons MW, Baron J-C. The ischemic penumbra: From concept to reality. Int J Stroke. 2021;16:497–509.

45. Jia J, Yang L, Chen Y, Zheng L, Chen Y, Xu Y, et al. The Role of Microglial Phagocytosis in Ischemic Stroke. Front Immunol. 2022;12.

46. Paolicelli RC, Sierra A, Stevens B, Tremblay M-E, Aguzzi A, Ajami B, et al. Microglia states and nomenclature: A field at its crossroads. Neuron. 2022;110:3458–83.

47. Cai W, Liu H, Zhao J, Chen LY, Chen J, Lu Z, et al. Pericytes in Brain Injury and Repair After Ischemic Stroke. Transl Stroke Res. 2017;8:107–21.

48. Wang, H., Li, X., Wang, Q., Ma, J., Gao, X., Wang, M. TREM2, microglial and ischemic stroke. J Neuroimmunol. 2023;381.

49. Pérez Falo C. Papel del neuropéptido cortistatina en la fisiopatología de los procesos de des- y remielinización en el sistema nervioso [Internet]. Universidad de Granada; 2021. Available from: https://dialnet.unirioja.es/servlet/tesis?codigo=295627

50. Neher JJ, Emmrich JV, Fricker M, Mander PK, Théry C, Brown GC. Phagocytosis executes delayed neuronal death after focal brain ischemia. Pro Natl Acad Sci. 2013;110:E4098–107.

51. Jolivel V, Bicker F, Binamé F, Ploen R, Keller S, Gollan R, et al. Perivascular microglia promote blood vessel disintegration in the ischemic penumbra. Acta Neuropathol. 2015;129:279–95.

52. Xu X, Gao W, Li L, Hao J, Yang B, Wang T, et al. Annexin A1 protects against cerebral ischemia–reperfusion injury by modulating microglia/macrophage polarization via FPR2/ALX-dependent AMPK-mTOR pathway. J Neuroinflammation. 2021;18:119.

53. Li Q, Barres BA. Microglia and macrophages in brain homeostasis and disease. Nat Rev Immunol. 2018;18:225–42.

54. Wen Q, Ding Q, Wang J, Yin Y, Xu S, Ju Y, et al. Cortistatin-14 Exerts Neuroprotective Effect Against Microglial Activation, Blood-brain Barrier Disruption, and Cognitive Impairment in Sepsis-associated Encephalopathy. J Immunol Res. 2022;2022:3334145.

1087 55. Han X, Liu Y-J, Liu B-W, Ma Z-L, Xia T-J, Gu X-P. TREM2 and CD163 Ameliorate
1088 Microglia-Mediated Inflammatory Environment in the Aging Brain. J Mol Neurosci.
1089 2022;72:1075–84.

1090 56. Roy-O'Reilly M, Zhu L, Atadja L, Torres G, Aronowski J, McCullough L, et al. Soluble
1091 CD163 in intracerebral hemorrhage: biomarker for perihematomal edema. Ann Clin Transl
1092 Neurol. 2017;4:793–800.

1093 57. Shen X-Y, Gao Z-K, Han Y, Yuan M, Guo Y-S, Bi X. Activation and Role of Astrocytes in
1094 Ischemic Stroke. Front Cell Neurosci. 2021;15.

1095 58. Burda JE, Sofroniew MV. Reactive Gliosis and the Multicellular Response to CNS Damage
1096 and Disease. Neuron. 2014;81:229–48.

1097 59. Zamanian JL, Xu L, Foo LC, Nouri N, Zhou L, Giffard RG, et al. Genomic Analysis of
1098 Reactive Astrogliosis. J Neurosci. 2012;32:6391–410.

1099 60. Liddelow SA, Barres BA. Reactive Astrocytes: Production, Function, and Therapeutic
1100 Potential. Immunity. 2017;46:957–67.

1101 61. Escartin C, Galea E, Lakatos A, O'Callaghan JP, Petzold GC, Serrano-Pozo A, et al.
1102 Reactive astrocyte nomenclature, definitions, and future directions. Nat Neurosci.
1103 2021;24:312–25.

1104 62. Karantali E, Kazis D, Papavasileiou V, Prevezianou A, Chatzikonstantinou S, Petridis F,
1105 et al. Serum BDNF Levels in Acute Stroke: A Systematic Review and Meta-Analysis. Medicina
1106 (Kaunas). 2021;57:297.

1107 63. Faulkner JR, Herrmann JE, Woo MJ, Tansey KE, Doan NB, Sofroniew MV. Reactive
1108 astrocytes protect tissue and preserve function after spinal cord injury. J Neurosci.
1109 2004;24:2143–55.

1110 64. Candelario-Jalil E, Dijkhuizen RM, Magnus T. Neuroinflammation, Stroke, Blood-Brain
1111 Barrier Dysfunction, and Imaging Modalities. Stroke. 2022;53:1473–86.

1112 65. Castillo-González J, Gonzalez-Rey E. Beyond wrecking a wall: Revisiting the concept of
1113 blood-brain barrier breakdown in ischemic stroke.Neural Regen Res. 2024;2.

1114 66. Bernardo-Castro S, Sousa JA, Brás A, Cecília C, Rodrigues B, Almendra L, et al.
1115 Pathophysiology of Blood–Brain Barrier Permeability Throughout the Different Stages of
1116 Ischemic Stroke and Its Implication on Hemorrhagic Transformation and Recovery. Front
1117 Neurol. 2020;11.

1118 67. Ballabh P, Braun A, Nedergaard M. The blood–brain barrier: an overview: Structure,
1119 regulation, and clinical implications. Neurobiol Dis. 2004;16:1–13.

1120 68. Fischer S, Wobben M, Marti HH, Renz D, Schaper W. Hypoxia-induced hyperpermeability
1121 in brain microvessel endothelial cells involves VEGF-mediated changes in the expression of
1122 zonula occludens-1. Microvasc Res. 2002;63:70–80.

1123 69. Sajja RK, Prasad S, Cucullo L. Impact of altered glycaemia on blood-brain barrier
1124 endothelium: an in vitro study using the hCMEC/D3 cell line. Fluids Barriers CNS. 2014;11:8.

1125 70. Famakin BM. The Immune Response to Acute Focal Cerebral Ischemia and Associated
1126 Post-stroke Immunodepression: A Focused Review. Aging Dis. 2014;5:307–26.

1127 71. Jayaraj RL, Azimullah S, Beiram R, Jalal FY, Rosenberg GA. Neuroinflammation: friend
1128 and foe for ischemic stroke. J Neuroinflammation. 2019;16:142.

1129 72. Grønhøj MH, Clausen BH, Fenger CD, Lambertsen KL, Finsen B. Beneficial potential of
1130 intravenously administered IL-6 in improving outcome after murine experimental stroke. Brain,
1131 Behav Immun. 2017;65:296–311.

1132 73. Gertz K, Kronenberg G, Kälin RE, Baldinger T, Werner C, Balkaya M, et al. Essential role
1133 of interleukin-6 in post-stroke angiogenesis. Brain. 2012;135:1964–80.

1134 74. Figiel I. Pro-inflammatory cytokine TNF-alpha as a neuroprotective agent in the brain. Acta
1135 Neurobiol Exp (Wars). 2008;68:526–34.

1136 75. Gonzalez-Rey, E., Varela, N., Sheibanie, A.F., Chorny, A., Ganea, D., Delgado, M.,
1137 Cortistatin, an antiinflammatory peptide with therapeutic action in inflammatory bowel
1138 disease. Proc Natl Acad Sci U S A. 2006;103, 4228–4233.

1139 76. Gonzalez-Rey E, Chorny A, Moral RGD, Varela N, Delgado M. Therapeutic effect of
1140 cortistatin on experimental arthritis by downregulating inflammatory and Th1 responses. Ann
1141 Rheum Dis. 2007;66:582–8.

1142 77. Andres RH, Choi R, Pendharkar AV, Gaeta X, Wang N, Nathan JK, et al. The CCR2/CCL2
1143 Interaction Mediates the Transendothelial Recruitment of Intravascularly Delivered Neural
1144 Stem Cells to the Ischemic Brain. Stroke. 2011;42:2923–31.

1145 78. Sippel TR, Shimizu T, Strnad F, Traystman RJ, Herson PS, Waziri A. Arginase I Release
1146 from Activated Neutrophils Induces Peripheral Immunosuppression in a Murine Model of
1147 Stroke. J Cereb Blood Flow Metab. 2015;35:1657–63.

1148 79. Barakat W, Fahmy A, Askar M, El-Kannishy S. Effectiveness of arginase inhibitors against
1149 experimentally induced stroke. Naunyn Schmiedebergs Arch Pharmacol. 2018;391:603–12.

1150 80. Tratsiakovich Y, Yang J, Gonon AT, Sjöquist P-O, Pernow J. Arginase as a target for
1151 treatment of myocardial ischemia-reperfusion injury. Eur J Pharmacol. 2013;720:121–3.

1152 81. Giordano R, Picu A, Bonelli L, Broglio F, Prodam F, Grottoli S, et al. The activation of
1153 somatostatinergic receptors by either somatostatin-14 or cortistatin-17 often inhibits ACTH
1154 hypersecretion in patients with Cushing's disease. Eur J Endocrinol. 2007;157:393–8.

1155 82. Grottoli S, Gasco V, Broglio F, Baldelli R, Ragazzoni F, Gallenca F, et al. Cortistatin-17
1156 and Somatostatin-14 Display the Same Effects on Growth Hormone, Prolactin, and Insulin
1157 Secretion in Patients with Acromegaly or Prolactinoma. J Clin Endocrinol Metab.
1158 2006;91:1595–9.

1159

1160